

1 **Deep cervical lymph nodes of patients with multiple sclerosis show**
2 **dysregulated B cells in the presence of Epstein-Barr virus**

3 **Authors:**

4 Joonas Sarkkinen^{1,*†}, Dawit Yohannes^{1,†}, Nea Kreivi¹, Pia Dürnsteiner¹, Jani
5 Huuhtanen¹⁻⁴, Kirsten Nowlan¹, Goran Kurdo⁵, Riikka Linden⁵, Mika Saarela⁶, Pentti J
6 Tienari^{1,6}, Eliisa Kekäläinen¹, Maria Perdomo⁷, Sini M Laakso^{1,6,*}

7
8 **Affiliations:**

9 ¹ Translational Immunology Research Program, University of Helsinki, Helsinki, Finland

10 ² Hematology Research Unit Helsinki, Department of Hematology, University of Helsinki
11 and Helsinki University Hospital Comprehensive Cancer Center, Helsinki, Finland

12 ³ ICAN Digital Precision Cancer Medicine Flagship, University of Helsinki and Helsinki
13 University Hospital Comprehensive Cancer Center, Helsinki, Finland

14 ⁴ Department of Computer Science, Aalto University School of Science, Espoo, Finland

15 ⁵ Department of Radiology, University of Helsinki and Helsinki University Hospital,
16 Helsinki, Finland

17 ⁶ Department of Neurology, Brain Center, Helsinki University Hospital, Helsinki, Finland

18 ⁷ Department of Virology, University of Helsinki and Helsinki University Hospital,
19 Helsinki, Finland

20 † Equal contribution

21 * Corresponding author

22

23 **Abstract:** Despite the recognized role of Epstein-Barr virus (EBV) in predisposing to
24 multiple sclerosis (MS) and the effectiveness of B cell-depleting therapies in MS, the
25 mechanism of autoimmunity remains elusive. Using fine needle aspirations, we
26 investigated deep cervical lymph nodes (dcLNs), the primary site of the adaptive
27 immune response against EBV, in newly diagnosed untreated MS patients and healthy
28 controls. We characterized the immune landscape of dcLNs with scRNAseq and CITE-
29 seq and observed increased memory B cell proportions and reduced germinal center
30 (GC) B cells with decreased clonality in patients with MS compared to healthy controls.
31 In the patient with an active MS relapse, we detected elevated plasmablasts, reduced
32 GC B cells, and clonally expanded memory CD8 T cells targeting EBV in the dcLN.
33 These findings, along with increased EBV DNA detection in dcLNs and viral loads in
34 patient saliva, support B cell dysregulation as a key mechanism in MS pathogenesis.
35
36

37 **INTRODUCTION**

38 Multiple sclerosis (MS) is the most common neurological autoimmune disease affecting
39 2.8 million individuals worldwide and has an increasing prevalence (1). Demyelinating
40 inflammatory lesions of the central nervous system (CNS) are the cause of clinical
41 attacks in relapsing-remitting MS (RRMS), which presents in 90% of patients, and
42 migration of lymphocytes to the CNS is the hallmark of the disease pathology (2).
43 Despite research efforts, the exact mechanisms that lead to MS remain unknown.

44
45 Several environmental and genetic risk factors that predispose to MS have been
46 observed, of which Epstein Barr Virus (EBV) infection in early adulthood is by far the
47 most significant. EBV infection is characterized by the proliferation and transformation of
48 infected B cells and the subsequent proliferation of CD8+ T cells targeting EBV. After
49 primary infection, EBV persists lifelong in a small subset of B cells (3). Close to 100% of
50 MS patients are EBV seropositive (4, 5), and recently, Bjornevik et al showed that EBV
51 infection in early adulthood raises the risk for MS by 32-fold (6). These epidemiological
52 findings were limited only to EBV, and seropositivity to other herpesviruses such as
53 cytomegalovirus (CMV) does not raise the risk for MS.

54
55 Antibodies recognizing EBV may cross-react with self-antigens (7). Recently, clonally
56 expanded intrathecal plasmablasts (PBs) were found to produce antibodies that bind to
57 EBV transcription factor EBNA1 but also to glial cell adhesion molecule (GlialCAM). In
58 addition, EBNA1 immunization of experimental autoimmune encephalitis (EAE) mice
59 exacerbated the EAE by increasing autoreactive B and T cell responses. (8) EBV-
60 targeting cytotoxic CD8+ T cells have also been detected in autopsy samples of
61 demyelinating brain lesions of MS patients. (9, 10)

62
63 The adaptive immune response against EBV occurs most importantly in the deep
64 cervical lymph nodes (dcLN) (11), which drain CNS lymphatics carrying neuronal
65 autoantigens also in MS patients (12–14). Interestingly, dcLNs are enlarged in MS
66 patients compared to healthy individuals (15), and clonally expanded B cells extracted
67 from the demyelinating lesions in MS patients commonly derive from the dcLNs (16).

68 Therefore, it is plausible that dcLN could be the original site where MS pathogenesis is
69 initiated.

70

71 These findings, together with the high efficacy of B cell-depleting therapies in treating
72 RRMS, have moved the MS research focus from T cells towards B cells and T-B cell
73 crosstalk. B cell responses are refined in germinal centers (GCs), where B cell somatic
74 hypermutations (SHMs) and class switching take place. GCs are typically found in
75 secondary lymphoid tissues, such as LNs. Ectopic GCs, which develop in response to
76 chronic inflammation (17), have also been found on the meninges of MS patients
77 possibly contributing to B cell autoreactivity in MS (16, 18). The GC reaction is regulated
78 by Tfr cells, whereas Tfh cells supply aid to developing B cells, which differentiate into
79 memory B cells (MBCs) and high-affinity antibody (ab) producing PBs and plasma cells
80 (PCs) (19). The ratio of follicular T helper cells (Tfh) to follicular regulator cells (Tfr) in
81 the circulation has been reported to be increased in MS and to correlate with intrathecal
82 IgG production, which suggests dysregulation of GC reactions (20).

83

84 We hypothesized that EBV infection disrupts B cell homeostasis and the GC
85 microenvironment in the dcLNs of MS patients, creating the ground for B cell-mediated
86 autoimmunity. Using fine needle aspirations (FNAs) of the dcLNs (21) in newly
87 diagnosed MS patients and healthy controls, we investigated the immunological
88 landscape of dcLNs at single-cell resolution focusing on the GC reaction. We show, for
89 the first time in an *ex vivo* analysis of MS patients, an intranodal expansion of memory B
90 cells and diminished GC B cell proportion and clonality, paralleled by EBV detection.
91 Our results reveal altered cellular composition of dcLNs in newly diagnosed MS
92 patients, providing insights into the role of EBV in disease pathogenesis and to the
93 efficacy of B cell depleting therapies in RRMS.

94

95

96 **RESULTS**

97 **Investigation of deep cervical lymph nodes accessed by fine needle aspirations**

98 Ultrasound-guided FNAs of dcLNs followed by isolation of viable single cells and
99 immediate processing for 5' single-cell RNA sequencing including T and B cell receptor
100 sequencing were performed on 7 MS patients (mean age 36 years, 4/9 females) and 6
101 healthy controls (mean age 28 years, 3/5 females, Fig. 1A). The width and height of
102 dcLNs, measured with ultrasound, did not differ between MS patients and controls
103 (median 0.53 vs 0.49 cm, t-test $p = 0.7024$; median 1.85 vs 1.26 cm, t-test $p = 0.1673$,
104 respectively). Hybrid-capture sequencing of DNA viruses (22) was performed on dcLN
105 FNAs, and blood and saliva were collected for further viral assays. Clinical features of
106 MS patients, including the Expanded Disability Status Scale (EDSS), are shown in
107 Table 1, and further information on study subjects and assays is presented in Data file
108 S1.

109
110 After excluding samples with an abnormally low number of cells due to reported technical
111 issues in 10x runs, scRNA-seq data from six MS patients and three healthy controls
112 containing a total of 73,074 cells, with an average of 8,195 cells per MS patient and 7,968
113 cells for the controls, were taken for further analysis. All cells were merged for combined
114 cluster analysis in Seurat (23), and the resulting clusters contained cells from each
115 sample without evident batch effect (Fig. 1B). We compared also cell clusters between
116 the batches (Data file S1) and observed that resulting clusters were well aligned across
117 library preparation and sequencing batches showing no specific batch effect (see
118 Methods and Fig. S1A-E) (24). We performed cell type determination using a combination
119 of automatic annotation with SingleR (25) using the Monaco reference (26) and manual
120 annotation aided by the CITE-seq data that we had for 4/6 MS patients and all (3/3)
121 healthy controls (Fig. 1C). Manual cell type determination was used especially for T and
122 B cell subsets using a combination of key markers on both transcript and protein levels
123 (Fig. 1D-E, Data file S2-3, see Supplementary Material for details). Most of the dcLN cells
124 were either T or B cells, whereas natural killer (NK) cell and myeloid cell subsets
125 accounted for less than 5% of all identified cells (Fig. 1F).

126

127 Two Tfh clusters were identified and characterized by canonical *CXCR5* expression (27),
128 of which the other cluster was in the minority ($\approx 0.5\%$ of all cells). Given the abundant
129 expression of *BCL6* (28), *ICOS* (29), *TOX2* (30), *PDCD1* (31), *SH2D1A* (*SAP*) (32), and
130 *IL21* (33), this smaller cluster likely represents a more active phenotype of Tfh (here GC
131 Tfh) cells interacting with GC B cells (34) (Fig. 1D, Data file S2). Instead, the other Tfh
132 cluster, which was the second most prevalent of all cells ($\approx 11\%$) after naïve CD4+ T cells
133 ($\approx 40\%$, Fig. 1F), could reside outside the GC given the lower *BCL6* expression (34, 35)
134 and was annotated as Tfh-like cells (Fig. 1D).

135 **Increased proportion of memory B cells and decreased GC B cells and GC Tfh** 136 **cells in dcLNs of MS patients**

137 We noted a significantly increased proportion of memory and a marginally elevated
138 proportion of naïve B cells in MS patients compared to healthy controls (unpaired t-test p
139 = 0.042 and log2 fold change ($\log_2\text{fc}$) = 0.88 for memory B cells; p = 0.064, $\log_2\text{fc}$ = 0.75
140 for naïve B cells, Fig. 1G, Data file S4). Next, we pooled all cells by subject group and
141 compared the overall cell type frequency distribution between MS patients and healthy
142 controls. The cell type frequencies, representing cellular compositions in dcLNs, were
143 significantly different between MS patients and controls (Pearson's Chi-squared test, p -
144 value $< 2.2\text{e-}16$). Furthermore, evaluation of the standardized Pearson residuals
145 suggests that in addition to memory and naïve B cells, PBs and Tfh-like cells were
146 significantly increased while naïve and intermediate CD4s, GC B cells, naïve CD8s, and
147 GC Tfh cells were significantly decreased in MS patients compared to healthy controls
148 (Fig. 1H, each having extreme standardized Pearson residual values above ± 3.65 ,
149 corresponding to Bonferroni corrected p -values < 0.00013 in the null distribution of the
150 standardized residuals). Tfr cells, which share transcriptional properties with Treg and Tfh
151 cells and differentially expressed *FOXP3*, *IKZF2*, *CTLA4* on transcript level and *PDCD1*,
152 and *ICOS* on both transcript and protein level (19, 36) (Data file S2-3), did not differ
153 between MS patients and healthy controls. Decreased GC B cells and GC Tfh cells
154 combined with a simultaneous expansion of memory B cells suggest an imbalance of the
155 GC reaction in MS.

156

157 We also conducted differential expression (DE) analysis for pseudobulked cell types. The
158 highest number of DE genes (DEG) in MS samples compared to controls were observed
159 in naïve CD4 T cells followed by plasmablasts, NK cells, and GC B cells (Fig. S1F, Data
160 file S5). In MS patients, plasmablasts upregulated several immunoglobulin (IG) heavy and
161 light chain genes compared to healthy controls. GC B cells upregulated *CCDN2* (*cyclin*
162 *D2*, $P_{\text{adj}} = 0.024$, $\log_2\text{fc} = 1.97$) and downregulated *LYN* ($P_{\text{adj}} = 0.024$, $\log_2\text{fc} = 0.93$) in
163 the MS group as compared to controls. *CCDN2* is upregulated during positive selection
164 in GCs (37), whereas loss of Lyn has been linked with a lupus-like autoimmune disease
165 with hyperactive B cells (38). Although statistically not significant, the expression of
166 canonical B cell marker *CD19*, known to regulate B cell proliferation in GC reaction (39),
167 was decreased in GC B cells of MS patients ($P_{\text{adj}} = 0.07$, $\log_2\text{fc} = -1.12$) in transcription
168 level, and also in protein level ($P_{\text{adj}} = 5.9\text{e-}18$, $\log_2\text{fc} = -0.47$) together with *CR1* ($P_{\text{adj}} =$
169 $6.7\text{e-}12$, $\log_2\text{fc} = -0.47$) and *CR2* ($P_{\text{adj}} = 1.4\text{e-}17$, $\log_2\text{fc} = -0.55$) (Fig. S1G). Interestingly,
170 the *CR1* and *CR2* expression on B cells is also decreased in systemic lupus
171 erythematosus and rheumatoid arthritis (40). Memory CD8+ T cells were upregulating an
172 IFN γ modulator *DKK3* (*Dickkopf-3*, $P_{\text{adj}} = 0.0015$, $\log_2\text{fc} 2.12$), *TIGIT* ($P_{\text{adj}} = 0.038$, $\log_2\text{fc}$
173 $= 0.59$), and cytotoxic granzymes A and K in MS patients compared to controls (*GZMA*,
174 $P_{\text{adj}} = 0.038$, $\log_2\text{fc} = 0.44$; *GZMB*, $P_{\text{adj}} = 0.0028$, $\log_2\text{fc} = 0.50$). *DKK3* is upregulated in
175 EAE (41) and *TIGIT* has been shown to promote CD8+ T cell exhaustion (42).

176

177 **Double-negative memory B cells are increased in MS patients**

178 To further characterize the B cell compartment where we found most differences in
179 abundance, we sub-clustered B cells. We identified similar B cell subsets as presented in
180 Fig. 1C, in addition to a T cell cluster initially clustered with memory and naïve B cells due
181 to a similar expression profile (Fig. S2A, Data file S6). The proportion of naïve B cells was
182 increased in MS dLNs after removing the remaining T cells ($p = 0.035$ and $\log_2\text{fc} = 0.82$,
183 Fig. S2B, Data file S7). Then we sub-clustered the memory and naïve B cells presented
184 in Fig. S2A and identified clusters of CD27 positive and IgD negative switched memory
185 (SM), CD27 and IgD positive unswitched memory (USM), and CD27 and IgD low double

186 negative (DN) B cells in addition to naïve B cells with the combination of both transcript
187 and protein level information (Fig. 2A-B, Fig. S2C, Data file S8). MS patients had elevated
188 proportions of the USM, SM, and naïve B cells, yet only the proportion of DN B cells was
189 significantly larger (% of B cells, $p = 0.041$ and $\log_2\text{fc} = 1.82$, Fig. 2C; % of all cells, $p =$
190 0.048 and $\log_2\text{fc} = 2.51$, Fig. S2D, Data file S9). Of note, DN B cells expressed less
191 CXCR5 than SM and USM B cells at both RNA and protein levels (Fig. 2B, Fig. S2C),
192 indicating that DN B cells could have been derived extrafollicularly (43, 44). Despite being
193 limited by cell numbers from dcLNs, in a subset of samples with higher cell yields, we
194 also performed flow cytometry analysis of the B cell compartment (see Methods, Fig.
195 S2E). We adapted the gating strategy from (45) and observed that the proportion of GC
196 B cells (CD19+CD20+CD38++CD10+IgD-) was reduced in MS patients compared to
197 controls and the proportions of memory (CD19+CD20+CD27+) and naïve
198 (CD19+CD20+IgD+CD27-CD38-) B cells were increased, however, due to the small
199 sample size, these results did not reach statistical significance (Fig. S2F). Moreover,
200 when dissecting the memory B cell compartment, the proportions of SM
201 (CD19+CD20+CD27+IgD-IgM-CD38-) and DN (CD19+CD20+CD27-IgD-IgM-CD38-) B
202 cells were higher in MS patients, however again without statistically significant difference
203 to healthy controls (Fig S2F). The flow cytometry results align with our findings from the
204 scRNAseq/CITEseq data, corroborating our observations of a larger memory B cell
205 compartment together with fewer GC B cells in the dcLNs of MS patients.

206

207 Next, we sub-clustered the GC B cells to study the GC reaction more thoroughly. We
208 identified *CD83* and *BCL2A1* expressing light zone (LZ) B cells (46, 47), *CXCR4*, *AICDA*,
209 and *MKI67* expressing dark zone (DZ1, DZ2) B cells (46, 47), and an unidentified GC B
210 cluster (GC.B) characterized with *MS4A1/CD20* and *MKI67* and negligible *CD3*
211 expression (Fig. 2D-F, Data file S10). Active proliferation is a defining characteristic of
212 GC B cells, and that is why no cell-cycle correction was performed and explains why the
213 sub-clustering of GC B cells also contained a small cluster of proliferative T cells (Fig.
214 2G). Supporting the imbalanced GC reaction, we noticed that within the B cell
215 compartment, the proportion of GC B cell subsets of all B cells showed a lower trend in
216 MS patients (Fig. S2G). Within GC B cells, the GC.B cluster was significantly increased

217 in MS dcLNs compared to healthy controls ($p = 0.011$ and $\log_2fc = 2.42$, Fig. 2G, Data
218 file S11). As expected, pathway analysis of cluster-defining DEGs ($P_{adj} < 0.05$) with GO
219 biological processes showed a significant over-representation of pathways related to B
220 cell activation and differentiation among upregulated genes of LZ B cells and replication
221 among those of DZ B cells. Interestingly, the GC.B cluster, which was increased in MS
222 patients, showed an over-representation of ribosomal genes related to viral transcription
223 and viral gene expression (Data file S1).

224

225 **Cellular interactions between follicular T cells and GC B cells**

226 Since MS patients had an increased proportion of naïve B cells, memory B cells, and
227 PBs, while GC B cell and GC Tfh proportions were decreased compared to healthy
228 controls, we hypothesized that the interaction between T and B cell subsets is altered.
229 To study intercellular interactions, we used NicheNet (48), which links transcripts of
230 ligands in sender cells to their transcript targets in the receiver cell. Principally
231 developing GC B cells rely on signals from Tfh via CD40 – CD40L interaction to
232 undergo SHM and class-switching (49). Similarly, the most active CD40 – CD40LG
233 interactions for GC B cells were predicted between GC Tfh and Tfh-like cells (Fig. 3A).
234 Integrins prolong interactions between T and B cells (50), and interestingly *CD40LG* –
235 *ITGB1* (integrin beta 1) interaction was observed only between GC Tfh and GC B cells
236 emphasizing their crosstalk in GCs. GC Tfh cells were the only CD4+ T cells which
237 interacted with GC B cells via *CD28* – *CD86* and *CD28* – *CD80*, of which the latter is
238 reported to be crucial for T-B interactions in GC responses (51). Contrary to our
239 hypothesis, the above interactions between GC B cells and Tfh cells were similar for MS
240 patients and controls when compared using MultiNicheNet (52) (Fig. S3A). We
241 observed a slight increase in *galactin-1 (LGALS1)* – *lectin receptor CD69* interaction
242 between GC B and Tfh cells in MS patients (Fig. S3A), of which galactin-1 is shown to
243 favour PB differentiation (53). We did not observe *IL21* – *IL21R* interaction between GC
244 B cells and GC Tfh cells, however, this could have been affected by the small
245 proportions of both cell subsets. Instead, *IL21* – *IL21R* interaction was increased
246 between GC Tfh and naïve B cells, suggesting that part of the naïve B cells could have

247 already been dedicated for the GC reaction (33) (Fig. 3A). In line with this, *CD40LG* –
248 *CD40* interaction between GC Tfh/Tfh-like cells and naïve B cells was decreased in MS
249 patients compared to GC B cells (Fig. S3A). The naïve B cells dedicated to the GC
250 reaction could potentially receive less necessary proliferative signals from Tfh cells in
251 MS patients, which could lead to an altered GC response.

252

253 The precise mechanisms of how Tfr cells control the GC reaction and selection of Tfh
254 and GC B cell clones are largely unknown. Here, Tfr cells were predicted to interact with
255 GC B cells via *CD28* – *CD80/CD86* (Fig. 3A), which is needed for Tfr differentiation
256 (54). We did not observe CTLA4-mediated inhibition of CD80/CD86 costimulatory
257 signals between Tfr and GC B cells, which has been thought to play a key role in the
258 regulation of GC reaction (55). B cell proliferation, memory responses, and CXCR5
259 expression of GC B cells are downregulated via HLA-G – *LILRB1* (also known as *ILT2*)
260 interaction between T and B cells (56). *B2M* (beta-2-microglobulin) constitutes the light
261 chain of HLA-G, and *B2M* – *LILRB1* interaction was predicted only between Tfr and GC
262 B cells (Fig. 3A). Possibly *B2M* – *LILRB1* interaction is one mechanism for Tfr cells to
263 regulate GC B cell development and thus, GC reaction.

264

265 **GC B cells are less clonal in dcLNs of MS patients**

266 We evaluated the BCR repertoire in dcLNs of MS patients and healthy controls. On
267 average, BCRs from 1400 cells per MS patient and 882 per healthy control sample were
268 obtained. We observed no difference in the diversity of the total BCR repertoire (Fig. 3B),
269 nor in the BCR diversity of naïve B cells, memory B cells, or plasmablasts between
270 patients and controls (Fig. S3B). However, the BCR diversity of GC B cells was
271 significantly higher in MS patients when compared to healthy controls (Fig. 3C). To
272 confirm this, we used the Lanz et al. (8) definition for BCR clonotypes (see Methods)
273 where we still observed significantly increased diversity only in the GC B cell compartment
274 of MS patients (Fig. S3C). In summary, while we could detect a lower proportion of GC B
275 cells in MS dcLNs (Fig. 1H), their standardized BCR diversity was higher than in healthy
276 controls.

277

278 **TCR repertoire in dcLNs is similar between MS patients and controls**

279 From T cells we obtained single-cell paired TCR $\alpha\beta$ data for an average of 6124 cells
280 per MS patient and 6702 for healthy control, corresponding to 5851 and 6384 average
281 unique TCR clonotypes, respectively (Fig. S3D). Comparison of TCR diversity in the
282 entire dcLN-paired-TCR $\alpha\beta$ repertoire, with and without downsampling to the same read-
283 depth, showed no statistical difference in TCR clonality between MS and healthy
284 controls (Fig. 3D). We also found no statistical difference in repertoire diversity within
285 specific T cell subpopulations between patients and controls (Fig. S3E). To determine
286 the possibility of more TCR sharing among MS patients, we also compared TCR amino
287 acid level overlap rates for every possible pair between patients and controls, however,
288 no evidence for increased TCR overlap in MS dcLNs was found (Fig. S3F).

289

290 Given the decreased GC B cell clonality and proportion in MS dcLNs, we examined
291 follicular T cells closer. Only a few TCRs of Tfh-like, GC Tfh, and Tfr cells were shared
292 with TCRs from other T cell subsets within each individual, with no difference between
293 MS patients and controls (Fig. S3G). Tfr cells shared TCR clones with both Treg (in 3/6
294 MS patients and 1/3 controls) and Tfh-like cells (in 1/6 MS patients and 1/3 controls),
295 indicating that Tfr cells had developed from both cell types. A trajectory analysis of the
296 scRNA-seq data from Tfh-like, GC Tfh, Tfr, and Treg cells using slingshot (57) showed
297 a single developmental trajectory encompassing from Tfh-like cells via GC Tfh and Tfr
298 to Treg cells, suggesting that Tfr cells had developed from both Tfh and Treg cells, in
299 line with recent findings (Fig. S3H) (58).

300

301 To compare the antigen-driven TCR repertoire in the patients' dcLNs to controls, we
302 scanned the VDJdb database for possible specificity of all our TCR $\alpha\beta$ amino acid
303 clonotypes using tcrdist3 (see Methods). Predicted T-cell-specificity was higher in MS
304 patients towards epitopes of M.tuberculosis in Naïve CD4s (p-value=0.03, log2fc = 0.5),
305 Influenza A (p-value = 0.003, log2fc = 3) and EBV (marginally with p-value = 0.08 & log2fc
306 = 0.56) in GC Tfh cells (Fig. S3I), however, these were insignificant after we filtered for

307 HLA restriction of target TCRs (retaining HLA class 2 restricted hits for CD4+ T cells, and
308 HLA class 1 restricted hits for CD8+ T cells).

309

310 **Higher coverages of EBV, HHV-6B and HHV-7 in dcLNs and viral loads of EBV in** 311 **the saliva of MS patients**

312 All MS patients were seropositive for EBV viral capsid antigen (VCA) IgG (9/9), whereas
313 only five of the six controls were EBV VCA IgG seropositive. Of the EBV VCA IgG
314 seropositive individuals, MS patients had higher EBV VCA IgG titer than healthy controls
315 ($p = 0.019$, Fig. S4A). None of the subjects were seropositive for EBV VCA IgM.

316

317 Next, by using hybrid-capture sequencing, we searched for common human DNA viruses
318 from fine needle aspirations of dcLNs ($n_{MS}=4$, $n_{hc}=4$, Fig. 1A). The prevalence of EBV
319 (75% vs 50%, human-herpesvirus-6B (HHV-6B, 50% vs 0%), and HHV-7 (100% vs 75%),
320 but also the total number of unique viral reads covering the reference sequences, which
321 correlates to the viral copy numbers (59), was higher in MS patients compared to controls
322 (Fig. 4A, Table 2). The coverages of HHV-7 were particularly higher in MS patients, from
323 whom we were able to reconstruct two near-complete viral genomes. Three out of four
324 MS patients were positive for parvovirus B19 (B19V) compared to 100% of controls. Equal
325 prevalence (50%) of Merkel cell polyomavirus was detected in both MS patients and
326 healthy controls. Importantly, MS patients and healthy controls clustered into separate
327 clusters based on the breadth coverage profiles of the above-tested viruses (Fig. 4A). We
328 aligned the scRNA-seq data to reference viral genomes available at ViruSITE (60) and
329 NCBI (61) databases (see Methods) including EBV genome to identify cells producing
330 viral transcripts (62). However, we did not find any cells producing transcripts of EBV, or
331 other herpesviruses.

332

333 Using multiplex qPCR HERQ-9 quantification we searched for EBV DNA from the saliva
334 as a sign of EBV reactivation. We found three out of nine HHVs in the saliva of MS patients
335 and controls: EBV, HHV-6B, and HHV-7. Herpes simplex virus-1 (HSV-1), HSV-2,
336 varicella-zoster virus, CMV, HHV-6A or Kaposi's sarcoma-associated herpesvirus were

337 not detected in any of the samples. EBV was found from saliva in all except one of the
338 MS patients in contrast to only one of the controls, and the viral loads in MS patients were
339 significantly higher ($p = 0.011$) (Fig. 4B). Surprisingly, the MS patient negative for EBV
340 DNA in dcLN had the highest EBV viral load in saliva. HHV-6B was found in most samples
341 and HHV-7 in all without significant differences in the viral loads for either of these viruses
342 between groups (Fig. S4B).

343

344 **Patient with an active MS relapse exhibits EBV targeting memory CD8 cells,** 345 **skewed follicular T cell ratios, and negligible GC B cells**

346 Immunological processes during active MS relapse are poorly understood, partly
347 because treatment is usually started soon after hospital admission. We managed to
348 obtain dcLN FNA from one patient during hospitalisation for an active MS relapse before
349 immunomodulatory treatments were started. The patient (MS011) had no other known
350 diseases besides MS nor an immediate history of infections and exhibited weakness of
351 the right leg and diplopia with EDSS of 3.5 in the clinical evaluation during the relapse
352 (Table 1). The patient's plasma EBV VCA IgG concentration and copy numbers of
353 HHVs in saliva were comparable to MS patients (Table 2).

354

355 When comparing cell abundancies from dcLNs, we observed that the patient had the
356 highest proportions of PBs, Tfh-like, and memory CD8 T cells, and the lowest
357 proportions of naïve, intermediate, and effector CD4, GC Tfh, Tfr, and GC B cells
358 across all subjects (Fig. 1G, Fig. S5A). The abundance of memory and naïve B cells
359 were similar to those in other patients. The ratio of GC Tfh to Tfh-like cells was reduced,
360 while the total Tfh to Tfr ratio was significantly increased (Fig. 5A), both likely due to the
361 drastic increase of Tfh-like cells (Fig. S5A). Moreover, the patient had the lowest
362 proportion of DZ and LZ B cells of all B cells. Within the GC B cell compartment the
363 cluster of GC.B cells, characterized by upregulation of transcripts involved in pathways
364 of viral transcription and viral gene expression, was significantly increased (Fig. 2G,
365 S2D, S5B).

366

367 We also redid analysis on cellular abundancies between patients and controls after
368 excluding the patient with acute exacerbation to evaluate how much of the results were
369 affected by the acute case. After excluding the acute relapse patient, non-treated MS
370 patients still had significantly increased memory and naïve B, and effector CD4 T cells,
371 decreased GC B, naïve CD4, and CD8, and intermediate CD4 T cells, and marginally
372 decreased GC Tfh cells (Fig. 5B). To conclude, the alterations of lymphocytes
373 characterized with larger memory B cell compartment and smaller proportion of GC B
374 cells in dcLNs seem more pronounced in early MS during a relapse.

375
376 The patient had the highest number of all BCRs and PB BCRs (Fig. 5C), whereas the
377 lowest of GC B cell BCRs (5 GC B cell BCRs of 1758 detected BCRs, detected BCRs in
378 all samples ranged from 599 to 1758). On the TCR side, while the relative frequency of
379 expanded T-cell clonotypes was not statistically different between the patient groups,
380 the largest percent of cells from expanded TCR clonotypes was seen in the patient with
381 relapse (1.16% of all T cell clonotypes were expanded, the median in MS patients is
382 0.40% and in controls 0.15%; paired TCR clonotypes with frequencies of over 0.001 of
383 all clonotypes within each sample were considered expanded), of which the most (84%)
384 were memory CD8 T cells (Fig. 5D). Notably, the majority of the clonally expanded T
385 cells from the patient were predicted to be EBV specific, whereas no EBV specific TCRs
386 were seen in T cells of other subjects (Fig. 5E). We validated and refined the TCR
387 predictions with an orthogonal method TCRGP, which has outperformed the original
388 tcrdist algorithm (63). With TCRGP, we confirmed the enrichment of clonally expanded
389 CD8+ TCR specific to EBV antigen EBNA3B in the patient with an active relapse (Fig.
390 S5C, $P_{\text{adj}} = 0.0002$, odds ratio (OR) = 18.80, Benjamini-Hochberg corrected one-sided
391 Fisher's exact test).

392 **DISCUSSION**

393 Therapeutic advances during the last decades have highlighted the role of B cells and
394 T-B crosstalk in MS pathogenesis. Examining B cell subsets at the site where B cell-
395 mediated immunity evolves is essential for gaining a deeper understanding of the origin
396 of MS and for elucidating why systemic B cell-depletion effectively treats the disease.
397 Here, to the best of our knowledge, we have provided the first-ever characterization of
398 the single-cell immune landscape in the dcLNs of newly diagnosed MS patients by
399 coupling scRNA-seq with CITE-seq. The B cell compartment of dcLNs is altered in MS
400 patients with an increase in memory B cells and decreased GC B cells with reduced
401 clonality suggesting a disturbance of GC reactions. Hybrid-capture sequencing of
402 eukaryotic DNA virome detected EBV, HHV-6B and HHV-7 DNA more readily in the
403 patients' dcLNs than the controls. Moreover, using multiplex qPCR from the saliva
404 against common herpesviruses, EBV DNA was witnessed primarily in the patients and
405 not the controls. In addition, the MS patient sampled during an acute relapse presented
406 with starker findings in the same B cell subsets together with clonally expanded memory
407 CD8+ T cells whose TCRs were likely targeting EBV.

408
409 Expansion of memory B cells and plasma cells in the CSF of MS patients is well
410 demonstrated (8, 16, 64). Simultaneously, Tfh cells are more prevalent both in CSF of
411 MS patients and in MS animal models, where Tfh cells promote B cell accumulation and
412 disease progression (64). Therapeutic effect of systemic B cell depletion is mirrored in
413 CSF by a decrease in memory B cells, which further underlines the role of B cell
414 dysregulation in MS. Based on studies with twins (65) or with paired CSF and blood
415 samples (64, 66) the B cell expansion is restricted to the CNS, whereas peripheral
416 blood reflects the B cell compartment inadequately. Even though the expanded memory
417 B cells are shown to derive from the dcLNs (16), the role of dcLNs in MS has been
418 largely unstudied. To enlighten this, we investigated the dcLNs in MS patients and
419 controls and discovered that the proportion of memory B cells and to a smaller degree
420 PBs was augmented in dcLNs of MS patients. This suggests that the reported
421 expansion of intrathecal B cells, plasma cells (64) and circulatory memory B cells in
422 early MS (67) derive from alterations of B cell maturation in the dcLNs. In addition, MS

423 patients had fewer and less clonal GC B cells further suggesting dysregulation in GC
424 reaction. Also, the Tfh cells likely representing GC-resident Tfh cells (34) interacting
425 with GC B cells due to expression of *BCL6* (28), *ICOS* (29), *TOX2* (30), *PDCD1* (31),
426 *SH2D1A* (*SAP*) (32) were decreased in MS patients. Tentatively, GC B cells could
427 receive less survival signals in the light zone from GC-resident Tfh cells leading to
428 favoring the B cell differentiation toward memory B cell fate over PB fate (49, 68) and to
429 GC contraction (69) in dcLNs of MS patients. This would subsequently explain the
430 decrease of GC B cells in MS patients. Interestingly, autoimmunity-linked DN (45) but
431 also switched-memory B cells were increased in MS patients. Both of them could
432 develop in extrafollicular responses of the lymph node, not only in GCs (43). On the
433 other hand, Tfh cell-proportions were skewed especially in the patient with a relapse, in
434 which Tfh-like cells, that probably remain outside the GC (GC-nonresident Tfh), were
435 expanded. Chronic viral infections seem to favour Tfh differentiation, yet result in
436 dysregulated Tfh – GC B cell interactions (79). Hence, local activation of latent EBV
437 could be a driver for the GC-nonresident Tfh expansion during the disease relapses
438 leading to a larger memory B cell compartment in MS patients as observed here.
439 Further studies on larger datasets with paired CSF samples are warranted to
440 demonstrate whether altered GC reaction in dcLNs is the origin of clonally expanded
441 intrathecal B cells in MS, potentially opening the door to new therapeutic strategies.

442

443 Epidemiological evidence for EBV infection as a prerequisite for MS onset is strong.
444 However, the exact pathogenic mechanisms leading to MS after this ubiquitous viral
445 infection are still unresolved. Molecular mimicry between CNS structures and EBV has
446 been widely acknowledged (8), but why such reactions lead to CNS autoimmunity in
447 only a minority of humans infected with EBV remains still unresolved. Findings of EBV
448 from postmortem samples have been contradicting (70–72), thus an uncontrolled viral
449 activation or replication as the cause of MS is still debatable. Interestingly, spontaneous
450 proliferation of CD4+ T cells initiated by memory B cells has been reported in MS
451 patients with HLA-DR15 haplotype (73) and is stimulated by EBV peptides (74).
452 Considering the observed expansion of memory B cells in MS dcLNs, EBV-infected B
453 cells could be the source of uncontrolled proliferation of CD4+ T cells.

454

455 Contrary to previous results by Gieß et al (75), we observed EBV DNA in the saliva of
456 adult early MS patients, possibly due to a more sensitive method. Similarly, oral
457 shedding of EBV as a possible sign of EBV lytic cycle reactivation has been reported in
458 pediatric MS patients (76). We detected EBV DNA in higher prevalence in MS patients
459 dcLNs than in controls, however, we could not find cells producing EBV nor other
460 aforementioned viruses by aligning scRNA-seq reads to viral genomes. Yet, it should be
461 noted that the copies of the viruses detected by hybrid-capture sequencing were likely
462 to be few, and the low efficiency of scRNA-seq library preparation (77) limits the
463 likelihood of detecting cells with viral transcripts from the scRNA-seq data. Our findings
464 of EBV activation lead us to speculate whether, in early MS, relapses could rise from
465 local activation of latent EBV in dcLNs, which would not be detected systematically with
466 serological assays (78). Recently, EBV-specific memory CD8⁺ T cells were observed in
467 CSF of both healthy controls and MS patients, however, patients' had also central
468 memory CD8⁺ T cells associated with broader EBV-specific repertoires (80). In our
469 study, the patient with an ongoing relapse had expanded EBV targeting memory CD8⁺
470 T cells, and it is possible that they expand and migrate to CNS during a relapse, since
471 this was not observed in patients without active relapses.

472

473 The understanding of GC reaction is largely based on experiments with mice, and
474 studies with human tissues, especially in autoimmunity are few since patient recruitment
475 and sample collection are challenging. Our dcLN data set from recently diagnosed MS
476 patients without immunosuppressive medication is unique, however, it is restricted with
477 the small sample size. Also, our scRNAseq experiments were limited to 10,000 cells per
478 sample, which impeded the T and B cell clonotype analysis. The majority of the VDJdb
479 database is based on CD8⁺ T cells, which could explain why we could not detect CD4⁺
480 T cell subsets targeting several viruses, such as EBV. Despite the limited cell number
481 per sample, we studied paired TCR $\alpha\beta$ data from an average of 6124 T cells per MS
482 patient and 6702 per healthy control, which increases the specificity of our clonotype
483 results. Yet, we did not find any differences in repertoire diversity within specific T-cell
484 subpopulations when comparing MS patients to healthy controls, which suggests that

485 clonal expansion of specific T cell clones unlikely dominates in dcLNs outside the MS
486 relapses. The only EBV-targeting T cells were clonally expanded memory CD8+ T cells
487 found only in the MS patient with a relapse. Using TCRGP, we confirmed that the
488 memory CD8+ TCRs in the patient with relapse were specific to latency-associated EBV
489 antigen EBNA3B (7) and increased 18.8 times compared to healthy controls.

490

491 Our results encourage the use of FNA and scRNAseq to study lymphoid tissues,
492 including ectopic GCs in autoimmune infiltrates, in various diseases to better
493 understand autoimmune mechanisms and development of memory B cells and
494 plasmablasts. By investigating the single-cell immune microenvironment of dcLNs at the
495 diagnosis of MS, we observe increased memory B cell compartment along with
496 decreased GC B cells in comparison to healthy controls, suggesting malfunction of the
497 GC reaction in the patients. Paralleled with findings related to EBV and the known
498 influence of EBV on GC dynamics (81), our results support B cell dysregulation as a key
499 mechanism in MS pathogenesis.

500

501 **MATERIALS AND METHODS**

502 **Study design**

503 We studied the cellular compartment of dcLNs in MS patients and healthy controls using
504 ultrasound-guided FNAs. Viable single cells were isolated from the FNAs and
505 subsequently processed for 5' single-cell RNA sequencing and hybrid-capture
506 sequencing of DNA viruses (22). Also, blood and saliva were collected from the
507 participants for additional viral assays.

508

509 This study was approved by the Helsinki University Hospital ethical committee (decision
510 number 5774/2020; research permit number 2363/2020). All subjects participated
511 voluntarily and gave written informed consent according to the principles of the
512 Declaration of Helsinki. Nine newly diagnosed MS patients and 7 age and sex-matched
513 healthy controls were selected for this study between April 2021 and March 2022. MS
514 diagnosis was confirmed by an experienced neurologist at the Helsinki University
515 Hospital using the 2017 McDonald diagnostic criteria (82, 83). The full diagnostic
516 workup included evaluation by a neuroimmunologist, CSF analysis, and a head MRI. All
517 MS patients had oligoclonal bands in CSF at the time of diagnosis. We only chose MS
518 patients without any immunomodulatory medications. In addition, an absence of
519 intravenous glucocorticoid infusion within 3 months before sample collection was a part
520 of the inclusion criteria. Further patient characteristics are shown in Data file S1.

521

522 **Sampling of blood and saliva**

523 Blood and saliva were taken 1 to 3 hours before the FNA sample. Blood samples were
524 collected into Li-heparin Vacutainer tubes (BD Biosciences), and plasma was separated
525 by centrifugation and archived at -80 C° until enzyme-linked immunosorbent assay
526 (ELISA). Subjects had a minimum of a 30-minute break from any liquids or solid foods
527 before saliva samples were obtained. The samples were collected at noon to normalize
528 the diurnal variation of protein secretion and stored at -20 C°. EBV serology status was

529 evaluated using Anti-EBV-CA ELISA IgG and IgM kits (Euroimmun, CAT#: EI 2791-
530 9601 G, EI 2791-9601 M) according to the manufacturer's instructions.

531 **Fine needle aspirations**

532 Ultrasound-guided FNAs of dcLNs and subsequent processing for single-cell
533 sequencing were performed as described previously by Turner et al (84). Briefly,
534 radiologists (G.K, R.L) first measured dcLNs (Table 1), after which they performed
535 FNAs under visualization with a 25-gauge needle. For each sample, 2 aspirations were
536 taken and collected into 3ml of 10% FBS in RPMI 1640 followed by three 0.5 ml rinses.
537 After one wash with 2% FBS and 0.5mM EDTA in PBS, red blood cells were eliminated
538 using 1ml of ACK lysis (Lonza) followed by another wash using PBS supplemented with
539 2% FBS and 0.5mM EDTA. Single-cell RNA sequencing was performed in
540 concentrations of 1×10^7 cells per ml in calcium- and magnesium-free PBS with 0.04%
541 BSA solely or in parallel with the cellular indexing of transcriptomes and epitopes by
542 sequencing (CITE-seq). CITE-seq staining was performed for a minimum of 500,000
543 cells using TotalSeq™-C Human Universal Cocktail (BioLegend, cat 399905) according
544 to the manual. For the samples in which solely scRNAseq was performed, 10,000 cells
545 were targeted for sequencing. For part of the samples (Data file S1), a flow cytometry
546 assay was also performed to characterize B cell subsets (described further). The
547 remaining cells were frozen in RNA Later (Thermo Fisher) according to the
548 manufacturer's instructions at -80 C° .

549

550 **Single-cell sequencing**

551 scRNAseq was performed for 7/9 MS and 5/7 healthy control dcLN FNA samples of
552 which CITE-seq was performed for 5 MS and all healthy control samples. FIMM Single-
553 Cell Analytics core center at the University of Helsinki performed 5'RNAseq run and
554 library preparation for scRNAseq, TCR $\alpha\beta$, and BCR libraries using the Chromium Single
555 Cell 5' (v2 Chemistry Dual Index) with Feature Barcoding technology for Cell Surface
556 Protein and Immune Receptor Mapping (CITE-seq) as instructed by the manufacturer
557 (10X Genomics).

558

559 The sequencing was started immediately after FNA sample preparation and libraries
560 were sequenced on Illumina NovaSeq 6000 system (read lengths 26bp (Read 1), 10bp
561 (i7 Index), 10bp (i5 Index), and 90bp (Read 2). The raw scRNAseq data were
562 processed using Cell Ranger (v 2.2.0) against the human genome GRCh38. TCR $\alpha\beta$
563 and BCR data were processed with Cell Ranger v_{dj} pipeline to generate single cell
564 V(D)J sequences and paired clonotype calling according to the manufacturer's
565 instructions.

566

567 **Single-cell RNA, CITE-seq, and scTCR & BCR data analysis**

568 Analysis of scRNAseq data was performed using Seurat (v4.1.1) in R (23). Initial QC was
569 performed separately for each sample in which cells in the top 2 percentile for
570 mitochondrial gene expression and in the top 1 percentile for the number of genes
571 detected were removed. Also, one MS sample and three healthy control samples with an
572 abnormally low number of cells due to technical issues in 10x runs were removed. The
573 remaining samples were combined for cluster analysis with the merge function in Seurat.
574 Uniform manifold approximation and projection (UMAP) was then performed in Seurat
575 using the top 50 principal components of the merged data. Graph-based clustering and
576 cluster labelling were performed with a resolution of 1 of the FindClusters function. The
577 resulting clusters were defined by cell types and were well mixed from all possible batches
578 (library and sequencing batches, Fig. S1A-D). In addition, no sample or patient group-
579 specific misalignment of cell clusters was observed (Fig. 1B, Fig. S1E), thus no batch
580 correction of the dataset was needed. Cell-level cell-type annotation was mainly
581 performed with the reference-based SingleR method (v1.10.0) (25) using the Monaco
582 immune data as a reference (26). The most frequent cell-level annotation was assigned
583 to each cluster, and cell clusters with the same annotation were readily combined. We
584 then confirmed and refined the cluster-level annotations manually using cluster markers
585 detected from the scRNA-seq and CITE-seq data (Fig. 1D-E) and annotated additional
586 cell types of interest (such as GC B cells, Tfh-like, GC Tfh, Tfr) that were missing in the
587 reference data for SingleR. We also performed sub-clustering of B cell subsets, for which

588 cluster annotations were performed manually based on cluster markers detected from the
589 scRNA-seq and CITE-seq data (Fig. 2, Data file S6,8,10).

590

591 We then used the cell clusters as defined by the annotation above for further analyses.
592 To identify differentially abundant cell types in MS, cell type composition was evaluated
593 between MS and control samples by comparing the proportion of the cell types in the two
594 conditions. Differential gene expression was identified for each cell type using the
595 pseudobulk approach, which has been reported to outperform other single-cell DE
596 methods (85), by sum aggregating the RNA counts of genes per cell type per sample,
597 and comparing the pseudobulk gene expression within each cell type between MS and
598 controls using DESeq2 (v1.36.0) (86). Biological pathway analysis was then performed
599 for each cell type using the pathway-express method (R package ROntoTools v2.24.0)
600 (87, 88).

601

602 Basic evaluation and comparison of immune single-cell level TCR and BCR repertoire
603 clonality/diversity and clonal overlap were done with scRepertoire (v1.6.0) (89) and in-
604 house custom R script. We scanned the VDJdb database (release 2022-03-30) (90) of
605 known TCR-epitope targets for possible specificity of our TCRs using tcrdist3 (v0.2.2)
606 (91), with a tcrdist3 distance of less or equal to 12 per alpha and beta chain (translating
607 to one amino acid mismatch per chain) used to assign possible targets for our TCRs.
608 This was done for paired TCRab, and the specificity profiles were compared between MS
609 patients and controls. For validation, TCRGP (1.0.0) (63) models were made for the 28
610 HLA class I-restricted epitopes from endemic viruses (CMV, EBV, Influenza A). For the
611 predictions, only CD8+ T cells were used and a threshold corresponding to a false positive
612 rate (FPR) of 5% was determined for each epitope separately from the receiver operating
613 characteristic (ROC) curves obtained from the cross-validation experiments, as described
614 previously. For BCRs, clonality definition in scRepertoire was used, i.e., BCRs using the
615 same V gene for both heavy and light chains (HC and LC), and that have >85% nucleotide
616 similarity in the HC and LC CDR3s (with normalized Levenshtein distance) were grouped
617 into one clonotype. For comparison with our results, we also used the clonotype definition
618 by Lanz et al. 2022 (8), i.e., sharing the same HC and LC V and J genes, and exhibiting

619 >70% amino acid identity within the HC and LC CDR3s (with normalized Levenshtein
620 distance).

621
622 Human leukocyte antigen (HLA) genotypes were predicted from the scRNA-seq data with
623 arcasHLA (92), which has recently been shown to have better accuracy than other similar
624 tools (93). The HLA-DR15 allele with the strongest risk for MS, HLA-DRB1*15:01(74),
625 was present in all (3/3) of the healthy controls and half (3/6) of the MS patients (Data file
626 S1), suggesting that the observed TCR/BCR repertoire changes in our MS patients are
627 more likely caused by other reasons than due to HLA-DR15 allele.

628 **Intercellular communication analysis**

629 We used the NicheNet package (v. 2.0.1) (48) to study differences in intercellular
630 communications between observed cell types. In each combination of sender and
631 receiver cell type, genes that were expressed in at least 10% of the sender/receiver cell
632 type population and present in the pre-built NicheNet prior ligand-receptor interaction
633 model were chosen as potential receptor and ligand genes. In addition to ligand activity
634 analysis, the ligands were prioritized based on condition-specificities of the ligands and
635 receptors across all cell types to highlight any ligands and receptors expressed
636 differentially between MS patients and controls. We visualized the top ligand-receptor
637 pairs for each sender-receiver cell type combination using the mushroom plot function
638 offered by NicheNet. In addition, the MultiNicheNet package (v. 1.0.3) (52) was used to
639 observe differences between controls and MS patients. For the analysis, we followed the
640 main steps in the MultiNicheNet vignette.

641 **Detection of viruses from scRNAseq data**

642 To detect any EBV-producing cells, we used the Vulture pipeline (62), which utilizes viral
643 and prokaryote genome files from the ViruSITE (60) and NCBI (61) databases along with
644 alignment tools to map 10x scRNA-seq reads to microbial genomes. Vulture was used
645 together with the CellRanger alignment tool to map the raw scRNA-seq data to the
646 microbial genomes. After performing QC on the mapped reads, we normalized the

647 obtained counts across each sample. This enabled comparing the counts of microbial
648 features across samples.

649 **Hybrid-capture sequencing of DNA viruses from dcLN FNAs**

650 The DNA was extracted using the QIAamp DNA Mini Kit (Qiagen), following the
651 manufacturer's protocol for tissue extraction. The extracts were eluted in 60 ul of AE
652 buffer and the DNA was mechanically fragmented with a Covaris E220 with a target
653 length of 200 nt. Subsequently, the libraries were prepared with the KAPA HyperPlus kit
654 (Roche) using unique Dual Index Adapters (Roche). Targeted enrichment of the viral
655 DNAs was performed using a custom panel of biotinylated RNA probes (Arbor
656 Biosciences) as described by Toppinen et al (22). Each sample was individually
657 enriched via two rounds of hybridization, following the manufacturer's recommendations
658 for low-input DNA (MyBaits v5 kit; Arbor Biosciences). The probes were 100 bp in
659 length and designed with 2X tiling. Kapa Universal Blockers (Roche) were used to block
660 unspecific binding to the adapters during hybridization.

661
662 During library preparation and viral enrichment, the libraries were amplified 3x13-25
663 cycles. The clean-up steps were performed with 1x KAPA HyperPure Beads (Roche).
664 The enriched libraries were quantified with the KAPA Library Quantification Kit (Roche)
665 using Stratagene 3005P qPCR System (Agilent) and pooled for sequencing on
666 NovaSeq 6000 (one lane, S4, PE151 kit; Illumina).

667

668 **Data analysis of hybrid-capture sequencing**

669 The data analysis was done with TRACESPipeLite, a streamlined version of
670 TRACESPipe (94). The paired-end reads were trimmed and collapsed with
671 AdapterRemoval, cutting ambiguous bases at the 5'/3' termini with quality scores below
672 or equal to two. Reads shorter than 20 bases were discarded. FALCON-meta was used
673 to find the highest similar reference from the NCBI viral database (95). The reads were
674 aligned with BWA (96) using a seed length of 1000 and a maximum diff of 0.01. Read
675 duplicates were removed with SAMtools (97) and the consensus sequences were

676 reconstructed with BCFtools (98). The coverage profiles were created with BEDtools
677 (99). When in low breadth coverage (< 10%), the individual reads were manually
678 inspected and confirmed by BLAST. The pipeline is freely available, under the MIT
679 license, at <https://github.com/viromelab/TRACESPipeLite>, along with the code (included
680 in the TRACESPipeLite repository).

681 **Quantitative multiplex PCR (qPCR) of saliva**

682 DNA extraction was optimized by adapting the protocol from Qiagen QIAamp DNA
683 Blood Mini Kit and Qiagen DNeasy Blood & Tissue Kit (Qiagen, Hilden, Germany) to get
684 the highest yield of DNA. Initially, 8 ml of phosphate-buffered saline (PBS) (Lonza,
685 Basel, Switzerland) was added to 2 ml of each saliva sample. The samples were then
686 centrifuged at 1800 g for 10 minutes. The pellet was resuspended in 180 µl ATL buffer
687 by pipetting up and down. The sample was pipetted into a new tube with 40 µl
688 proteinase K, vortexed, and incubated at 56°C with shaking for 1 h. After this, 200 µl AL
689 buffer was added followed by vortex and incubation at 70°C for 10s min. From here, the
690 protocol continued following the Qiagen QIAamp DNA Blood Mini Kit Spin Protocol. In
691 the last step, DNA was eluted into 60 µl AE buffer with an incubation time of 5 min. The
692 samples were stored at -20°C until further processing.

693
694 Multiplex qPCR method HERQ-9 was used to detect and quantify nine HHVs
695 simultaneously from the saliva samples as described earlier by Pyöriä et al (100).
696 Briefly, HERQ-9 is designed in three triplex-qPCR reactions, the first one amplifying
697 herpes simplex viruses 1 and 2 (HSV-1 and 2) and varicella-zoster virus (VZV), the
698 second one amplifying EBV, human cytomegalovirus (HCMV), and Kaposi's sarcoma-
699 associated herpesvirus (KSHV), and the third one amplifying HHV-6A, -6B, and -7. The
700 viral loads were normalized per 10⁶ cells, determined with the human single-copy gene
701 RNase P qPCR (101).

702 **Flow cytometry**

703 For cell surface staining, cells were suspended in an antibody cocktail containing
704 LIVE/DEAD® Fixable Green Dead Cell Stain (ThermoFisher), which was prepared

705 using Brilliant Stain Buffer (BD Biosciences). The cell suspension was then incubated at
706 +4°C for 30 minutes and subsequently washed twice with FACS staining buffer (PBS,
707 pH 7.4, 10% FBS, and 2 mM EDTA). Flow cytometry data were acquired with LSR
708 Fortessa (BD Biosciences) and analyzed with FlowJo (BD Biosciences, LLC). Detailed
709 information about the antibodies used in this study can be found in Data file S13.

710 **Statistics**

711 Either the t-test or evaluation of the standardized Pearson residuals using the Chi-
712 Square test was used to compare two different categories. In the chi-squared test, all
713 cells were pooled by subject group and the overall cell type distribution frequency of the
714 standardized Pearson residuals was compared between MS patients and healthy
715 controls. Euclidean dissimilarity distances and either Ward's or complete agglomerative
716 clustering were used in the correlation plots. In differentially expressing markers (both
717 scRNA-seq and CITE-seq) analysis, the non-parametric Wilcoxon rank sum test was
718 used and adjustments for multiple testing were performed with Bonferroni correction.
719 Nominal and adjusted p-values (P_{adj}) of less than 0.05 were considered significant. In
720 the box plots, the vertical line corresponds to the median, the box corresponds to the
721 interquartile range (IQR), and the whiskers are $1.5 \times$ the IQR. All calculations were done
722 with R (4.2.1, 4.3.1) or Python (3.7.4).

723 **Supplementary Materials**

724 Supplementary Material on cluster phenotyping

725 Supplementary Figures 1-5

726 Description of supplementary datafiles

727

728 **References**

- 729 1. C. Walton, R. King, L. Rechtman, W. Kaye, E. Leray, R. A. Marrie, N. Robertson, N.
730 La Rocca, B. Uitdehaag, I. van der Mei, M. Wallin, A. Helme, C. Angood Napier, N.
731 Rijke, P. Baneke, Rising prevalence of multiple sclerosis worldwide: Insights from
732 the Atlas of MS, third edition. *Mult. Scler.* **26**, 1816–1821 (2020).
- 733 2. J. M. Fletcher, S. J. Lalor, C. M. Sweeney, N. Tubridy, K. H. G. Mills, T cells in
734 multiple sclerosis and experimental autoimmune encephalomyelitis. *Clin. Exp.*
735 *Immunol.* **162**, 1–11 (2010).
- 736 3. O. L. Hatton, A. Harris-Arnold, S. Schaffert, S. M. Krams, O. M. Martinez, The
737 interplay between Epstein-Barr virus and B lymphocytes: implications for infection,
738 immunity, and disease. *Immunol. Res.* **58**, 268–276 (2014).
- 739 4. S. Abrahamyan, B. Eberspächer, M.-M. Hoshi, L. Aly, F. Luessi, S. Groppa, L.
740 Klotz, S. G. Meuth, C. Schroeder, T. Grüter, B. Tackenberg, F. Paul, F. Then-
741 Bergh, T. Kümpfel, F. Weber, M. Stangel, A. Bayas, B. Wildemann, C. Heesen, U.
742 Zettl, C. Warnke, G. Antony, N. Hessler, H. Wiendl, S. Bittner, B. Hemmer, R. Gold,
743 A. Salmen, K. Ruprecht, German Competence Network Multiple Sclerosis
744 (KKNMS), Other members of the KKNMS that acted as collaborators in this study,
745 Complete Epstein-Barr virus seropositivity in a large cohort of patients with early
746 multiple sclerosis. *J. Neurol. Neurosurg. Psychiatry.* **91**, 681–686 (2020).
- 747 5. R. Dobson, J. Kuhle, J. Middeldorp, G. Giovannoni, Epstein-Barr-negative MS: a
748 true phenomenon? *Neurol Neuroimmunol Neuroinflamm.* **4**, e318 (2017).
- 749 6. K. Bjornevik, M. Cortese, B. C. Healy, J. Kuhle, M. J. Mina, Y. Leng, S. J. Elledge,
750 D. W. Niebuhr, A. I. Scher, K. L. Munger, A. Ascherio, Longitudinal analysis reveals
751 high prevalence of Epstein-Barr virus associated with multiple sclerosis. *Science*
752 (2022), doi:10.1126/science.abj8222.
- 753 7. S. S. Soldan, P. M. Lieberman, Epstein-Barr virus and multiple sclerosis. *Nat. Rev.*
754 *Microbiol.* **21**, 51–64 (2023).
- 755 8. T. V. Lanz, R. C. Brewer, P. P. Ho, J.-S. Moon, K. M. Jude, D. Fernandez, R. A.
756 Fernandes, A. M. Gomez, G.-S. Nadj, C. M. Bartley, R. D. Schubert, I. A. Hawes,
757 S. E. Vazquez, M. Iyer, J. B. Zuchero, B. Teegen, J. E. Dunn, C. B. Lock, L. B.
758 Kipp, V. C. Cotham, B. M. Ueberheide, B. T. Aftab, M. S. Anderson, J. L. DeRisi, M.
759 R. Wilson, R. J. M. Bashford-Rogers, M. Platten, K. C. Garcia, L. Steinman, W. H.
760 Robinson, Clonally Expanded B Cells in Multiple Sclerosis Bind EBV EBNA1 and
761 GlialCAM. *Nature* (2022), doi:10.1038/s41586-022-04432-7.
- 762 9. D. F. Angelini, B. Serafini, E. Piras, M. Severa, E. M. Coccia, B. Rosicarelli, S.
763 Ruggieri, C. Gasperini, F. Buttari, D. Centonze, R. Mechelli, M. Salvetti, G.
764 Borsellino, F. Aloisi, L. Battistini, Increased CD8+ T cell response to Epstein-Barr
765 virus lytic antigens in the active phase of multiple sclerosis. *PLoS Pathog.* **9**,
766 e1003220 (2013).

- 767 10. G. P. van Nierop, J. Mautner, J. G. Mitterreiter, R. Q. Hintzen, G. M. G. M. Verjans,
768 Intrathecal CD8 T-cells of multiple sclerosis patients recognize lytic Epstein-Barr
769 virus proteins. *Mult. Scler.* **22**, 279–291 (2016).
- 770 11. M. Abdel-Aziz, H. El-Hoshy, M. Rashed, M. Qotb, S. Awad, N. Naguib, Epstein-Barr
771 virus infection as a cause of cervical lymphadenopathy in children. *Int. J. Pediatr.*
772 *Otorhinolaryngol.* **75**, 564–567 (2011).
- 773 12. B. A. Plog, M. Nedergaard, The Glymphatic System in Central Nervous System
774 Health and Disease: Past, Present, and Future. *Annu. Rev. Pathol.* **13**, 379–394
775 (2018).
- 776 13. M. S. Albayram, G. Smith, F. Tufan, I. S. Tuna, M. Bostancıoğlu, M. Zile, O.
777 Albayram, Non-invasive MR imaging of human brain lymphatic networks with
778 connections to cervical lymph nodes. *Nat. Commun.* **13**, 203 (2022).
- 779 14. M. van Zwam, R. Huizinga, M.-J. Melief, A. F. Wierenga-Wolf, M. van Meurs, J. S.
780 Voerman, K. P. H. Biber, H. W. G. M. Boddeke, U. E. Höpken, C. Meisel, A. Meisel,
781 I. Bechmann, R. Q. Hintzen, B. A. 't Hart, S. Amor, J. D. Laman, L. A. Boven, Brain
782 antigens in functionally distinct antigen-presenting cell populations in cervical lymph
783 nodes in MS and EAE. *J. Mol. Med.* **87**, 273–286 (2009).
- 784 15. F. Di Giuliano, M. Albanese, E. Picchi, F. Mori, F. Buttari, G. A. Marfia, F. Garaci,
785 N. B. Mercuri, R. Floris, D. Centonze, S. Marziali, Abnormal cervical lymph nodes in
786 multiple sclerosis: a preliminary ultrasound study. *Radiol. Med.* **123**, 202–208
787 (2018).
- 788 16. J. N. H. Stern, G. Yaari, J. A. Vander Heiden, G. Church, W. F. Donahue, R. Q.
789 Hintzen, A. J. Huttner, J. D. Laman, R. M. Nagra, A. Nylander, D. Pitt, S. Ramanan,
790 B. A. Siddiqui, F. Vigneault, S. H. Kleinstein, D. A. Hafler, K. C. O'Connor, B cells
791 populating the multiple sclerosis brain mature in the draining cervical lymph nodes.
792 *Sci. Transl. Med.* **6**, 248ra107-248ra107 (2014).
- 793 17. C. Gago da Graça, L. G. M. van Baarsen, R. E. Mebius, Tertiary Lymphoid
794 Structures: Diversity in Their Development, Composition, and Role. *J. Immunol.*
795 **206**, 273–281 (2021).
- 796 18. O. W. Howell, C. A. Reeves, R. Nicholas, D. Carassiti, B. Radotra, S. M.
797 Gentleman, B. Serafini, F. Aloisi, F. Roncaroli, R. Magliozzi, R. Reynolds,
798 Meningeal inflammation is widespread and linked to cortical pathology in multiple
799 sclerosis. *Brain.* **134**, 2755–2771 (2011).
- 800 19. M. Stebegg, S. D. Kumar, A. Silva-Cayetano, V. R. Fonseca, M. A. Linterman, L.
801 Graca, Regulation of the Germinal Center Response. *Front. Immunol.* **9**, 2469
802 (2018).
- 803 20. M. Puthenparampil, A. Zito, G. Pantano, L. Federle, E. Stropparo, S. Miante, G. De
804 Silvestro, M. Plebani, P. Gallo, Peripheral imbalanced TFH/TFR ratio correlates

- 805 with intrathecal IgG synthesis in multiple sclerosis at clinical onset. *Mult. Scler.*
806 **2018/06/09**, 1352458518779951 (2018).
- 807 21. C. Havenar-Daughton, I. G. Newton, S. Y. Zare, S. M. Reiss, B. Schwan, M. J. Suh,
808 F. Hasteh, G. Levi, S. Crotty, Normal human lymph node T follicular helper cells
809 and germinal center B cells accessed via fine needle aspirations. *J. Immunol.*
810 *Methods.* **479**, 112746 (2020).
- 811 22. M. Toppinen, D. Pratas, E. Väisänen, M. Söderlund-Venermo, K. Hedman, M. F.
812 Perdomo, A. Sajantila, The landscape of persistent human DNA viruses in femoral
813 bone. *Forensic Sci. Int. Genet.* **48**, 102353 (2020).
- 814 23. Y. Hao, S. Hao, E. Andersen-Nissen, W. M. Mauck 3rd, S. Zheng, A. Butler, M. J.
815 Lee, A. J. Wilk, C. Darby, M. Zager, P. Hoffman, M. Stoeckius, E. Papalexi, E. P.
816 Mimitou, J. Jain, A. Srivastava, T. Stuart, L. M. Fleming, B. Yeung, A. J. Rogers, J.
817 M. McElrath, C. A. Blish, R. Gottardo, P. Smibert, R. Satija, Integrated analysis of
818 multimodal single-cell data. *Cell.* **184**, 3573-3587.e29 (2021).
- 819 24. M. Büttner, Z. Miao, F. A. Wolf, S. A. Teichmann, F. J. Theis, A test metric for
820 assessing single-cell RNA-seq batch correction. *Nat. Methods.* **16**, 43–49 (2019).
- 821 25. D. Aran, A. P. Looney, L. Liu, E. Wu, V. Fong, A. Hsu, S. Chak, R. P. Naikawadi, P.
822 J. Wolters, A. R. Abate, A. J. Butte, M. Bhattacharya, Reference-based analysis of
823 lung single-cell sequencing reveals a transitional profibrotic macrophage. *Nat.*
824 *Immunol.* **20**, 163–172 (2019).
- 825 26. G. Monaco, B. Lee, W. Xu, S. Mustafah, Y. Y. Hwang, C. Carré, N. Burdin, L.
826 Visan, M. Ceccarelli, M. Poidinger, A. Zippelius, J. Pedro de Magalhães, A. Larbi,
827 RNA-Seq Signatures Normalized by mRNA Abundance Allow Absolute
828 Deconvolution of Human Immune Cell Types. *Cell Rep.* **26**, 1627-1640.e7 (2019).
- 829 27. P. Schaerli, K. Willmann, A. B. Lang, M. Lipp, P. Loetscher, B. Moser, CXC
830 chemokine receptor 5 expression defines follicular homing T cells with B cell helper
831 function. *J. Exp. Med.* **192**, 1553–1562 (2000).
- 832 28. D. Yu, S. Rao, L. M. Tsai, S. K. Lee, Y. He, E. L. Sutcliffe, M. Srivastava, M.
833 Linterman, L. Zheng, N. Simpson, J. I. Ellyard, I. A. Parish, C. S. Ma, Q.-J. Li, C. R.
834 Parish, C. R. Mackay, C. G. Vinuesa, The transcriptional repressor Bcl-6 directs T
835 follicular helper cell lineage commitment. *Immunity.* **31**, 457–468 (2009).
- 836 29. Y. S. Choi, R. Kageyama, D. Eto, T. C. Escobar, R. J. Johnston, L. Monticelli, C.
837 Lao, S. Crotty, ICOS receptor instructs T follicular helper cell versus effector cell
838 differentiation via induction of the transcriptional repressor Bcl6. *Immunity.* **34**, 932–
839 946 (2011).
- 840 30. W. Xu, X. Zhao, X. Wang, H. Feng, M. Gou, W. Jin, X. Wang, X. Liu, C. Dong, The
841 Transcription Factor Tox2 Drives T Follicular Helper Cell Development via
842 Regulating Chromatin Accessibility. *Immunity.* **51**, 826-839.e5 (2019).

- 843 31. J. Shi, S. Hou, Q. Fang, X. Liu, X. Liu, H. Qi, PD-1 Controls Follicular T Helper Cell
844 Positioning and Function. *Immunity*. **49**, 264-274 e4 (2018).
- 845 32. J. Hu, C. Havenar-Daughton, S. Crotty, Modulation of SAP dependent T:B cell
846 interactions as a strategy to improve vaccination. *Curr. Opin. Virol.* **3**, 363–370
847 (2013).
- 848 33. A. R. Dvorscek, C. I. McKenzie, M. J. Robinson, Z. Ding, C. Pitt, K. O'Donnell, D.
849 Zotos, R. Brink, D. M. Tarlinton, I. Quast, IL-21 has a critical role in establishing
850 germinal centers by amplifying early B cell proliferation. *EMBO Rep.* **23**, e54677
851 (2022).
- 852 34. C.-H. Yeh, J. Finney, T. Okada, T. Kurosaki, G. Kelsoe, Primary germinal center-
853 resident T follicular helper cells are a physiologically distinct subset of CXCR5hiPD-
854 1hi T follicular helper cells. *Immunity*. **55**, 272-289.e7 (2022).
- 855 35. S. T. Kim, J.-Y. Choi, B. Lainez, V. P. Schulz, D. E. Karas, E. D. Baum, J. Setlur, P.
856 G. Gallagher, J. Craft, Human Extrafollicular CD4+ Th Cells Help Memory B Cells
857 Produce Igs. *J. Immunol.* **201**, 1359–1372 (2018).
- 858 36. V. Panneton, B. C. Mindt, Y. Bouklouch, A. Bouchard, S. Mohammaei, J. Chang, N.
859 Diamantopoulos, M. Witalis, J. Li, A. Stancescu, J. E. Bradley, T. D. Randall, J. H.
860 Fritz, W.-K. Suh, ICOS costimulation is indispensable for the differentiation of T
861 follicular regulatory cells. *Life Sci Alliance*. **6** (2023), doi:10.26508/lsa.202201615.
- 862 37. L. Mesin, J. Ersching, G. D. Victora, Germinal Center B Cell Dynamics. *Immunity*.
863 **45**, 471–482 (2016).
- 864 38. C. Lamagna, Y. Hu, A. L. DeFranco, C. A. Lowell, B cell-specific loss of Lyn kinase
865 leads to autoimmunity. *J. Immunol.* **192**, 919–928 (2014).
- 866 39. Y. Wang, R. H. Carter, CD19 regulates B cell maturation, proliferation, and positive
867 selection in the FDC zone of murine splenic germinal centers. *Immunity*. **22**, 749–
868 761 (2005).
- 869 40. A. Erdei, K. G. Kovács, Z. Nagy-Baló, S. Lukácsi, B. Mácsik-Valent, I. Kurucz, Z.
870 Bajtay, New aspects in the regulation of human B cell functions by complement
871 receptors CR1, CR2, CR3 and CR4. *Immunol. Lett.* **237**, 42–57 (2021).
- 872 41. M. Meister, M. Papatriantafyllou, V. Nordström, V. Kumar, J. Ludwig, K. O. Lui, A.
873 S. Boyd, Z. V. Popovic, T. H. Fleming, G. Moldenhauer, P. P. Nawroth, H.-J.
874 Gröne, H. Waldmann, T. Oelert, B. Arnold, Dickkopf-3, a tissue-derived modulator
875 of local T-cell responses. *Front. Immunol.* **6**, 78 (2015).
- 876 42. R. J. Johnston, L. Comps-Agrar, J. Hackney, X. Yu, M. Huseni, Y. Yang, S. Park,
877 V. Javinal, H. Chiu, B. Irving, D. L. Eaton, J. L. Grogan, The immunoreceptor TIGIT
878 regulates antitumor and antiviral CD8(+) T cell effector function. *Cancer Cell*. **26**,
879 923–937 (2014).

- 880 43. R. A. Elsner, M. J. Shlomchik, Germinal Center and Extrafollicular B Cell
881 Responses in Vaccination, Immunity, and Autoimmunity. *Immunity*. **53**, 1136–1150
882 (2020).
- 883 44. S. A. Jenks, K. S. Cashman, E. Zumaquero, U. M. Marigorta, A. V. Patel, X. Wang,
884 D. Tomar, M. C. Woodruff, Z. Simon, R. Bugrovsky, E. L. Blalock, C. D. Scharer, C.
885 M. Tipton, C. Wei, S. S. Lim, M. Petri, T. B. Niewold, J. H. Anolik, G. Gibson, F. E.-
886 H. Lee, J. M. Boss, F. E. Lund, I. Sanz, Distinct Effector B Cells Induced by
887 Unregulated Toll-like Receptor 7 Contribute to Pathogenic Responses in Systemic
888 Lupus Erythematosus. *Immunity*. **49**, 725-739.e6 (2018).
- 889 45. I. Sanz, C. Wei, S. A. Jenks, K. S. Cashman, C. Tipton, M. C. Woodruff, J. Hom, F.
890 E.-H. Lee, Challenges and Opportunities for Consistent Classification of Human B
891 Cell and Plasma Cell Populations. *Front. Immunol.* **10**, 2458 (2019).
- 892 46. D. Morgan, V. Tergaonkar, Unraveling B cell trajectories at single cell resolution.
893 *Trends Immunol.* **43**, 210–229 (2022).
- 894 47. P. Milpied, I. Cervera-Marzal, M.-L. Mollichella, B. Tesson, G. Brisou, A. Traverse-
895 Glehen, G. Salles, L. Spinelli, B. Nadel, Human germinal center transcriptional
896 programs are de-synchronized in B cell lymphoma. *Nat. Immunol.* **19**, 1013–1024
897 (2018).
- 898 48. R. Browaeys, W. Saelens, Y. Saeys, NicheNet: modeling intercellular
899 communication by linking ligands to target genes. *Nat. Methods.* **17**, 159–162
900 (2020).
- 901 49. G. D. Victora, M. C. Nussenzweig, Germinal Centers. *Annu. Rev. Immunol.* **40**,
902 413–442 (2022).
- 903 50. A. Biram, N. Davidzohn, Z. Shulman, T cell interactions with B cells during germinal
904 center formation, a three-step model. *Immunol. Rev.* **288**, 37–48 (2019).
- 905 51. K. L. Good-Jacobson, E. Song, S. Anderson, A. H. Sharpe, M. J. Shlomchik, CD80
906 expression on B cells regulates murine T follicular helper development, germinal
907 center B cell survival, and plasma cell generation. *J. Immunol.* **188**, 4217–4225
908 (2012).
- 909 52. R. Browaeys, J. Gilis, C. Sang-Aram, P. De Bleser, L. Hoste, S. Tavernier, D.
910 Lambrechts, R. Seurinck, Y. Saeys, MultiNicheNet: a flexible framework for
911 differential cell-cell communication analysis from multi-sample multi-condition
912 single-cell transcriptomics data. *bioRxiv* (2023), p. 2023.06.13.544751, ,
913 doi:10.1101/2023.06.13.544751.
- 914 53. N. Giovannone, L. K. Smith, B. Treanor, C. J. Dimitroff, Galectin-Glycan
915 Interactions as Regulators of B Cell Immunity. *Front. Immunol.* **9**, 2839 (2018).

- 916 54. M. A. Linterman, W. Pierson, S. K. Lee, A. Kallies, S. Kawamoto, T. F. Rayner, M.
917 Srivastava, D. P. Divekar, L. Beaton, J. J. Hogan, S. Fagarasan, A. Liston, K. G. C.
918 Smith, C. G. Vinuesa, Foxp3⁺ follicular regulatory T cells control the germinal
919 center response. *Nat. Med.* **17**, 975–982 (2011).
- 920 55. V. R. Fonseca, F. Ribeiro, L. Graca, T follicular regulatory (Tfr) cells: Dissecting the
921 complexity of Tfr-cell compartments. *Immunol. Rev.* **288**, 112–127 (2019).
- 922 56. A. Naji, C. Menier, F. Morandi, S. Agaugué, G. Maki, E. Ferretti, S. Bruel, V.
923 Pistoia, E. D. Carosella, N. Rouas-Freiss, Binding of HLA-G to ITIM-bearing Ig-like
924 transcript 2 receptor suppresses B cell responses. *J. Immunol.* **192**, 1536–1546
925 (2014).
- 926 57. W. Saelens, R. Cannoodt, H. Todorov, Y. Saeys, A comparison of single-cell
927 trajectory inference methods. *Nat. Biotechnol.* **37**, 547–554 (2019).
- 928 58. C. Le Coz, D. A. Oldridge, R. S. Herati, N. De Luna, J. Garifallou, E. Cruz Cabrera,
929 J. P. Belman, D. Poeschl, L. V. Silva, A. V. C. Knox, W. Reid, S. Yoon, K. B. Zur, S.
930 D. Handler, H. Hakonarson, E. J. Wherry, M. Gonzalez, N. Romberg, Human T
931 follicular helper clones seed the germinal center-resident regulatory pool. *Sci*
932 *Immunol.* **8**, eade8162 (2023).
- 933 59. L. Pyöriä, D. Pratas, M. Toppinen, K. Hedman, A. Sajantila, M. F. Perdomo,
934 Unmasking the tissue-resident eukaryotic DNA virome in humans. *Nucleic Acids*
935 *Res.* **51**, 3223–3239 (2023).
- 936 60. M. Stano, G. Beke, L. Klucar, viruSITE—integrated database for viral genomics.
937 *Database* . **2016**, baw162 (2016).
- 938 61. E. W. Sayers, E. E. Bolton, J. R. Brister, K. Canese, J. Chan, D. C. Comeau, R.
939 Connor, K. Funk, C. Kelly, S. Kim, T. Madej, A. Marchler-Bauer, C. Lanczycki, S.
940 Lathrop, Z. Lu, F. Thibaud-Nissen, T. Murphy, L. Phan, Y. Skripchenko, T. Tse, J.
941 Wang, R. Williams, B. W. Trawick, K. D. Pruitt, S. T. Sherry, Database resources of
942 the national center for biotechnology information. *Nucleic Acids Res.* **50**, D20–D26
943 (2022).
- 944 62. J. Chen, D. Yin, H. Y. H. Wong, X. Duan, K. H. O. Yu, J. W. K. Ho, Vulture: Cloud-
945 enabled scalable mining of microbial reads in public scRNA-seq data. *bioRxiv*
946 (2023), p. 2023.02.13.528411, , doi:10.1101/2023.02.13.528411.
- 947 63. E. Jokinen, J. Huuhtanen, S. Mustjoki, M. Heinonen, H. Lähdesmäki, Predicting
948 recognition between T cell receptors and epitopes with TCRGP. *PLoS Comput.*
949 *Biol.* **17**, e1008814 (2021).
- 950 64. D. Schafflick, C. A. Xu, M. Hartlehnert, M. Cole, A. Schulte-Mecklenbeck, T.
951 Lautwein, J. Wolbert, M. Heming, S. G. Meuth, T. Kuhlmann, C. C. Gross, H.
952 Wiendl, N. Yosef, G. Meyer Zu Horste, Integrated single cell analysis of blood and
953 cerebrospinal fluid leukocytes in multiple sclerosis. *Nat. Commun.* **11**, 247 (2020).

- 954 65. F. Ingelfinger, L. A. Gerdes, V. Kavaka, S. Krishnarajah, E. Friebel, E. Galli, P.
955 Zwicky, R. Furrer, C. Peukert, C.-A. Dutertre, K. M. Eglseer, F. Ginhoux, A. Flierl-
956 Hecht, T. Kümpfel, D. De Feo, B. Schreiner, S. Mundt, M. Kerschensteiner, R.
957 Hohlfeld, E. Beltrán, B. Becher, Twin study reveals non-heritable immune
958 perturbations in multiple sclerosis. *Nature*. **603**, 152–158 (2022).
- 959 66. A. Ramesh, R. D. Schubert, A. L. Greenfield, R. Dandekar, R. Loudermilk, J. J.
960 Sabatino Jr, M. T. Koelzer, E. B. Tran, K. Koshal, K. Kim, A.-K. Pröbstel, D. Banerji,
961 University of California, San Francisco MS-EPIC Team, C.-Y. Guo, A. J. Green, R.
962 M. Bove, J. L. DeRisi, J. M. Gelfand, B. A. C. Cree, S. S. Zamvil, S. E. Baranzini, S.
963 L. Hauser, M. R. Wilson, A pathogenic and clonally expanded B cell transcriptome
964 in active multiple sclerosis. *Proc. Natl. Acad. Sci. U. S. A.* **117**, 22932–22943
965 (2020).
- 966 67. J. Leffler, S. Trend, N. C. Ward, G. E. Grau, S. Hawke, S. N. Byrne, A. G.
967 Kermode, M. A. French, P. H. Hart, Circulating Memory B Cells in Early Multiple
968 Sclerosis Exhibit Increased IgA+ Cells, Globally Decreased BAFF-R Expression
969 and an EBV-Related IgM+ Cell Signature. *Front. Immunol.* **13**, 812317 (2022).
- 970 68. R. Shinnakasu, T. Inoue, K. Kometani, S. Moriyama, Y. Adachi, M. Nakayama, Y.
971 Takahashi, H. Fukuyama, T. Okada, T. Kurosaki, Regulated selection of germinal-
972 center cells into the memory B cell compartment. *Nat. Immunol.* **17**, 861–869
973 (2016).
- 974 69. T. Arulraj, S. C. Binder, M. Meyer-Hermann, Investigating the Mechanism of
975 Germinal Center Shutdown. *Front. Immunol.* **13**, 922318 (2022).
- 976 70. L. A. Vella, R. S. Herati, E. J. Wherry, CD4(+) T Cell Differentiation in Chronic Viral
977 Infections: The Tfh Perspective. *Trends Mol. Med.* **23**, 1072–1087 (2017).
- 978 71. B. Serafini, B. Rosicarelli, D. Franciotta, R. Magliozzi, R. Reynolds, P. Cinque, L.
979 Andreoni, P. Trivedi, M. Salvetti, A. Faggioni, F. Aloisi, Dysregulated Epstein-Barr
980 virus infection in the multiple sclerosis brain. *J. Exp. Med.* **204**, 2899–2912 (2007).
- 981 72. S. N. Willis, C. Stadelmann, S. J. Rodig, T. Caron, S. Gattenloehner, S. S. Mallozzi,
982 J. E. Roughan, S. E. Almendinger, M. M. Blewett, W. Brück, D. A. Hafler, K. C.
983 O'Connor, Epstein-Barr virus infection is not a characteristic feature of multiple
984 sclerosis brain. *Brain*. **132**, 3318–3328 (2009).
- 985 73. L. A. N. Peferoen, F. Lamers, L. N. R. Lodder, W. H. Gerritsen, I. Huitinga, J.
986 Melief, G. Giovannoni, U. Meier, R. Q. Hintzen, G. M. G. M. Verjans, G. P. van
987 Nierop, W. Vos, R. M. B. Peferoen-Baert, J. M. Middeldorp, P. van der Valk, S.
988 Amor, Epstein Barr virus is not a characteristic feature in the central nervous
989 system in established multiple sclerosis. *Brain*. **133** (2010), p. e137.
- 990 74. I. Jelcic, F. Al Nimer, J. Wang, V. Lentsch, R. Planas, I. Jelcic, A. Madjovski, S.
991 Ruhrmann, W. Faigle, K. Frauenknecht, C. Pinilla, R. Santos, C. Hammer, Y. Ortiz,
992 L. Opitz, H. Grönlund, G. Rogler, O. Boyman, R. Reynolds, A. Lutterotti, M.

- 993 Khademi, T. Olsson, F. Piehl, M. Sospedra, R. Martin, Memory B Cells Activate
994 Brain-Homing, Autoreactive CD4+ T Cells in Multiple Sclerosis. *Cell*. **175**, 85-
995 100.e23 (2018).
- 996 75. J. Wang, I. Jelcic, L. Mühlenbruch, V. Haunerding, N. C. Toussaint, Y. Zhao, C.
997 Cruciani, W. Faigle, R. Naghavian, M. Foege, T. M. C. Binder, T. Eiermann, L.
998 Opitz, L. Fuentes-Font, R. Reynolds, W. W. Kwok, J. T. Nguyen, J.-H. Lee, A.
999 Lutterotti, C. Münz, H.-G. Rammensee, M. Hauri-Hohl, M. Sospedra, S. Stevanovic,
1000 R. Martin, HLA-DR15 Molecules Jointly Shape an Autoreactive T Cell Repertoire in
1001 Multiple Sclerosis. *Cell*. **183**, 1264-1281.e20 (2020).
- 1002 76. R. M. Gieß, C. Pfuhl, J. R. Behrens, L. Rasche, E. Freitag, N. Khalighy, C. Otto, J.
1003 Wuerfel, A. U. Brandt, J. Hofmann, B. Eberspächer, J. Bellmann-Strobl, F. Paul, K.
1004 Ruprecht, Epstein-Barr virus antibodies in serum and DNA load in saliva are not
1005 associated with radiological or clinical disease activity in patients with early multiple
1006 sclerosis. *PLoS One*. **12**, e0175279 (2017).
- 1007 77. C. Yea, R. Tellier, P. Chong, G. Westmacott, R. A. Marrie, A. Bar-Or, B. Banwell,
1008 Canadian Pediatric Demyelinating Disease Network, Epstein-Barr virus in oral
1009 shedding of children with multiple sclerosis. *Neurology*. **81**, 1392–1399 (2013).
- 1010 78. T. M. Yamawaki, D. R. Lu, D. C. Ellwanger, D. Bhatt, P. Manzanillo, V. Arias, H.
1011 Zhou, O. K. Yoon, O. Homann, S. Wang, C.-M. Li, Systematic comparison of high-
1012 throughput single-cell RNA-seq methods for immune cell profiling. *BMC Genomics*.
1013 **22**, 66 (2021).
- 1014 79. Ø. Torkildsen, H. Nyland, H. Myrmed, K.-M. Myhr, Epstein-Barr virus reactivation
1015 and multiple sclerosis. *Eur. J. Neurol*. **15**, 106–108 (2008).
- 1016 80. T. Schneider-Hohendorf, L. A. Gerdes, B. Pignolet, R. Gittelmann, P. Ostkamp, F.
1017 Rubelt, C. Raposo, B. Tackenberg, M. Riepenhausen, C. Janoschka, C. Wunsch,
1018 F. Bucciarelli, A. Flierl-Hecht, E. Beltrán, T. Kümpfel, K. Anslinger, C. C. Gross, H.
1019 Chapman, I. Kaplan, D. Brassat, H. Wekerle, M. Kerschensteiner, L. Klotz, J. D.
1020 Lünemann, R. Hohlfeld, R. Liblau, H. Wiendl, N. Schwab, Broader Epstein-Barr
1021 virus-specific T cell receptor repertoire in patients with multiple sclerosis. *J. Exp.*
1022 *Med*. **219** (2022), doi:10.1084/jem.20220650.
- 1023 81. E. D. SoRelle, N. M. Reinoso-Vizcaino, G. Q. Horn, M. A. Luftig, Epstein-Barr virus
1024 perpetuates B cell germinal center dynamics and generation of autoimmune-
1025 associated phenotypes in vitro. *Front. Immunol*. **13**, 1001145 (2022).
- 1026 82. A. J. Thompson, B. L. Banwell, F. Barkhof, W. M. Carroll, T. Coetzee, G. Comi, J.
1027 Correale, F. Fazekas, M. Filippi, M. S. Freedman, K. Fujihara, S. L. Galetta, H. P.
1028 Hartung, L. Kappos, F. D. Lublin, R. A. Marrie, A. E. Miller, D. H. Miller, X.
1029 Montalban, E. M. Mowry, P. S. Sorensen, M. Tintoré, A. L. Traboulsee, M. Trojano,
1030 B. M. J. Uitdehaag, S. Vukusic, E. Waubant, B. G. Weinshenker, S. C. Reingold, J.
1031 A. Cohen, Diagnosis of multiple sclerosis: 2017 revisions of the McDonald criteria.
1032 *Lancet Neurol*. **17**, 162–173 (2018).

- 1033 83. C. H. Polman, S. C. Reingold, B. Banwell, M. Clanet, J. A. Cohen, M. Filippi, K.
1034 Fujihara, E. Havrdova, M. Hutchinson, L. Kappos, F. D. Lublin, X. Montalban, P.
1035 O'Connor, M. Sandberg-Wollheim, A. J. Thompson, E. Waubant, B. Weinshenker,
1036 J. S. Wolinsky, Diagnostic criteria for multiple sclerosis: 2010 revisions to the
1037 McDonald criteria. *Ann. Neurol.* **69**, 292–302 (2011).
- 1038 84. J. S. Turner, J. Q. Zhou, J. Han, A. J. Schmitz, A. A. Rizk, W. B. Alsoussi, T. Lei, M.
1039 Amor, K. M. McIntire, P. Meade, S. Strohmeier, R. I. Brent, S. T. Richey, A. Haile,
1040 Y. R. Yang, M. K. Klebert, T. Suessen, S. Teefey, R. M. Presti, F. Krammer, S. H.
1041 Kleinstein, A. B. Ward, A. H. Ellebedy, Human germinal centres engage memory
1042 and naive B cells after influenza vaccination. *Nature.* **586**, 127–132 (2020).
- 1043 85. J. W. Squair, M. Gautier, C. Kathe, M. A. Anderson, N. D. James, T. H. Hutson, R.
1044 Hudelle, T. Qaiser, K. J. E. Matson, Q. Barraud, A. J. Levine, G. La Manno, M. A.
1045 Skinnider, G. Courtine, Confronting false discoveries in single-cell differential
1046 expression. *Nat. Commun.* **12**, 5692 (2021).
- 1047 86. M. I. Love, W. Huber, S. Anders, Moderated estimation of fold change and
1048 dispersion for RNA-seq data with DESeq2. *Genome Biol.* **15**, 550 (2014).
- 1049 87. S. Draghici, P. Khatri, A. L. Tarca, K. Amin, A. Done, C. Voichita, C. Georgescu, R.
1050 Romero, A systems biology approach for pathway level analysis. *Genome Res.* **17**,
1051 1537–1545 (2007).
- 1052 88. C. Voichita, M. Donato, S. Draghici, "Incorporating Gene Significance in the Impact
1053 Analysis of Signaling Pathways" in *2012 11th International Conference on Machine
1054 Learning and Applications* (2012), vol. 1, pp. 126–131.
- 1055 89. N. Borchering, N. L. Bormann, G. Kraus, scRepertoire: An R-based toolkit for
1056 single-cell immune receptor analysis. *F1000Res.* **9**, 47 (2020).
- 1057 90. M. Shugay, D. V. Bagaev, I. V. Zvyagin, R. M. Vroomans, J. C. Crawford, G.
1058 Dolton, E. A. Komech, A. L. Sycheva, A. E. Koneva, E. S. Egorov, A. V. Eliseev, E.
1059 Van Dyk, P. Dash, M. Attaf, C. Rius, K. Ladell, J. E. McLaren, K. K. Matthews, E. B.
1060 Clemens, D. C. Douek, F. Luciani, D. van Baarle, K. Kedzierska, C. Kesmir, P. G.
1061 Thomas, D. A. Price, A. K. Sewell, D. M. Chudakov, VDJdb: a curated database of
1062 T-cell receptor sequences with known antigen specificity. *Nucleic Acids Res.* **46**,
1063 D419–D427 (2018).
- 1064 91. K. Mayer-Blackwell, S. Schattgen, L. Cohen-Lavi, J. C. Crawford, A. Souquette, J.
1065 A. Gaevert, T. Hertz, P. G. Thomas, P. Bradley, A. Fiore-Gartland, TCR meta-
1066 clonotypes for biomarker discovery with tcrdist3 enabled identification of public,
1067 HLA-restricted clusters of SARS-CoV-2 TCRs. *Elife.* **10**, e68605 (2021).
- 1068 92. R. Orenbuch, I. Filip, D. Comito, J. Shaman, I. Pe'er, R. Rabadan, arcashLA: high-
1069 resolution HLA typing from RNAseq. *Bioinformatics.* **36**, 33–40 (2020).

- 1070 93. B. D. Solomon, H. Zheng, L. W. Dillon, J. D. Goldman, C. S. Hourigan, J. R. Heath,
1071 P. Khatri, Prediction of HLA genotypes from single-cell transcriptome data. *Front.*
1072 *Immunol.* **14**, 1146826 (2023).
- 1073 94. D. Pratas, M. Toppinen, L. Pyöriä, K. Hedman, A. Sajantila, M. F. Perdomo, A
1074 hybrid pipeline for reconstruction and analysis of viral genomes at multi-organ level.
1075 *Gigascience.* **9** (2020), doi:10.1093/gigascience/giaa086.
- 1076 95. D. Pratas, M. Hosseini, G. Grilo, A. J. Pinho, R. M. Silva, T. Caetano, J. Carneiro,
1077 F. Pereira, Metagenomic Composition Analysis of an Ancient Sequenced Polar
1078 Bear Jawbone from Svalbard. *Genes* . **9** (2018), doi:10.3390/genes9090445.
- 1079 96. H. Li, R. Durbin, Fast and accurate long-read alignment with Burrows-Wheeler
1080 transform. *Bioinformatics.* **26**, 589–595 (2010).
- 1081 97. H. Li, B. Handsaker, A. Wysoker, T. Fennell, J. Ruan, N. Homer, G. Marth, G.
1082 Abecasis, R. Durbin, 1000 Genome Project Data Processing Subgroup, The
1083 Sequence Alignment/Map format and SAMtools. *Bioinformatics.* **25**, 2078–2079
1084 (2009).
- 1085 98. H. Li, A statistical framework for SNP calling, mutation discovery, association
1086 mapping and population genetical parameter estimation from sequencing data.
1087 *Bioinformatics.* **27**, 2987–2993 (2011).
- 1088 99. A. R. Quinlan, *Curr. Protoc. Bioinformatics*, in press.
- 1089 100. L. Pyöriä, M. Jokinen, M. Toppinen, H. Salminen, T. Vuorinen, V.
1090 Hukkanen, C. Schmotz, E. Elbasani, P. M. Ojala, K. Hedman, H. Välimaa, M. F.
1091 Perdomo, HERQ-9 Is a New Multiplex PCR for Differentiation and Quantification of
1092 All Nine Human Herpesviruses. *mSphere.* **5** (2020), doi:10.1128/mSphere.00265-
1093 20.
- 1094 101. L. Pyöriä, M. Toppinen, E. Mäntylä, L. Hedman, L.-M. Aaltonen, M. Vihinen-
1095 Ranta, T. Ilmarinen, M. Söderlund-Venermo, K. Hedman, M. F. Perdomo, Extinct
1096 type of human parvovirus B19 persists in tonsillar B cells. *Nat. Commun.* **8**, 14930
1097 (2017).
- 1098

1099 **Acknowledgments:**

1100 We are grateful for the patients and healthy controls for their participation, and without
1101 whom this study would not have been possible. We thank Marjo Rissanen and Kalla-
1102 Maria Tiilikainen for their help with sample processing. The authors would like to thank
1103 the FIMM Single-Cell Analytics unit supported by HiLIFE and Biocenter Finland for
1104 scRNA and CITE-seq services.

1105

1106 **Funding:**

1107 Academy of Finland grant 332186 (SML)

1108 Competitive Research Funding of the State of Finland governed through Helsinki

1109 University Hospital grant TYH2020317 (SML)

1110 Finska Läkaresällskapet (SML)

1111 Suomen MS-Säätiö (JS)

1112 Emil Aaltonen Foundation (JS)

1113 Instrumentarium Science Foundation (JS)

1114 Suomen Lääketieteen säätiö grant 6006 (MP)

1115 Liv och Hälsa (MP)

1116

1117 **Author contributions:**

1118 Conceptualization: SML, JS, MP, EK, PJT

1119 Methodology: JS, DY, SML

1120 Software: DY, JH

1121 Validation: JS, DY, MP

1122 Formal Analysis: JS, DY, NK, PD, JH, MP

1123 Investigation: JS, PD, KN, GK, RL, MP, SML

1124 Resources: SML, MS, EK, MP

1125 Data Curation: JS, DY, NK, PD, KN, MP

1126 Writing – Original Draft: JS, DY, NK, SML

1127 Writing – Review & Editing: SML, JS, DY, JH, KN, PJT, EK, MP

1128 Visualization: JS, DY, NK, JH

1129 Supervision: EK, SML

1130 Project administration: JS, SML
1131 Funding acquisition: SML, EK, MP

1132

1133 **Competing interests:**

1134 SML: lecture fees Argenx, Biogen, Janssen, Merck, Novartis, Roche; congress
1135 expenses Merck, Novartis; advisory fee Argenx, Novartis, Roche, Sanofi, UCB Pharma;
1136 investigator for the clinical study Clarion (Merck) and sub-investigator for the clinical
1137 study Fenhance (Roche)

1138 PJT: Congress expenses Biogen, Novartis, Merck KGaA, Teva; fees for lectures
1139 Biogen, Roche, Novartis, Sanofi-Genzyme, Merck, Teva, Orion, Santen, Alexion.

1140

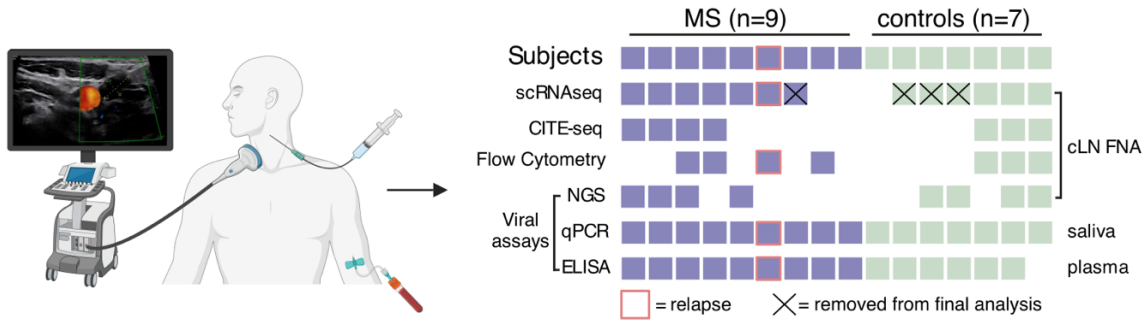
1141 **Data and materials availability:**

1142 The Seurat-objects of the processed scRNA-sequencing data including TCR and BCR
1143 and CITE-seq data are available at Zenodo (10.5281/zenodo.10006020) with restricted
1144 access due to GDPR regulations and data can be accessed by placing a request via
1145 Zenodo. Differentially expressed gene sets are available in supplementary data files.

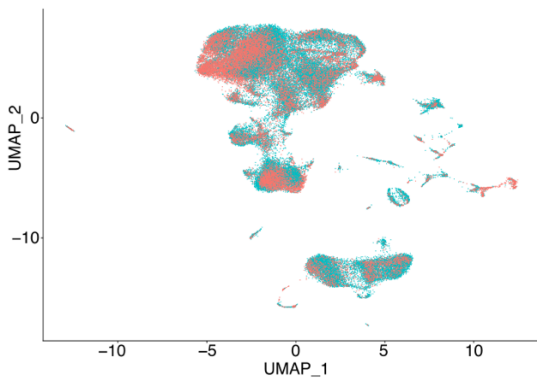
1146 The reconstructed near-complete HHV-7 genomes are available at GenBank
1147 (OR634979 and OR634980). The code to reproduce the key findings is available on
1148 GitHub (https://github.com/SarkkinenJ/cervical_lymphnodes_MS.git).

1149

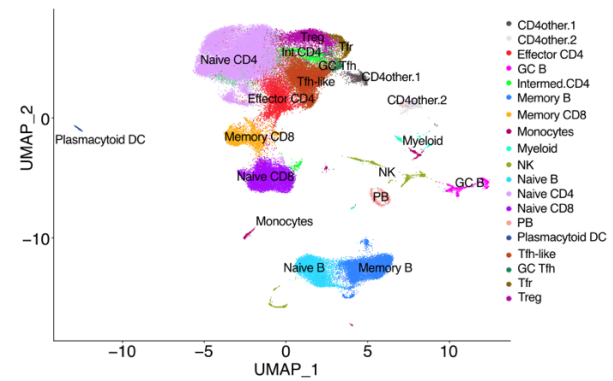
A.



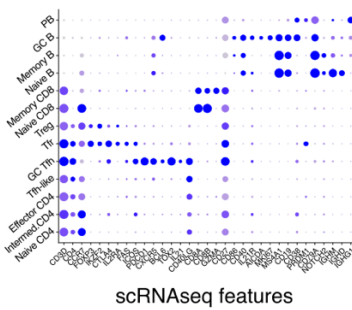
B.



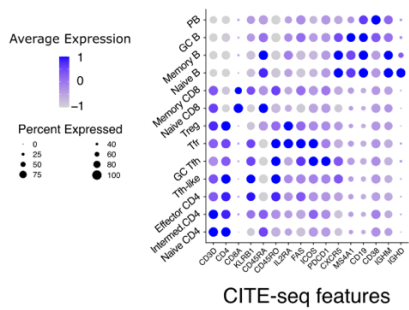
C.



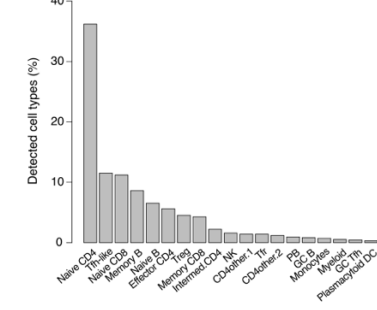
D.



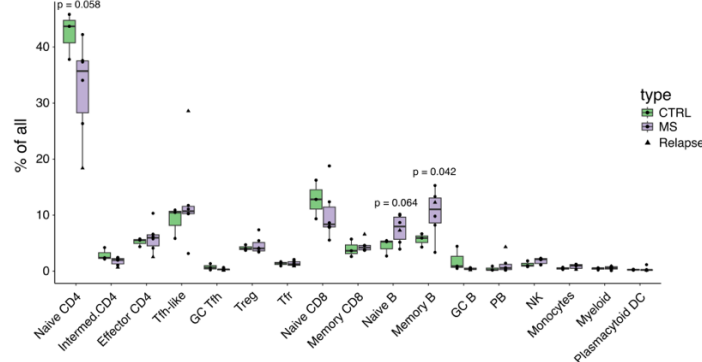
E.



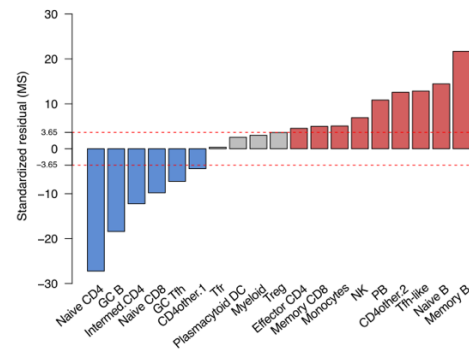
F.



G.



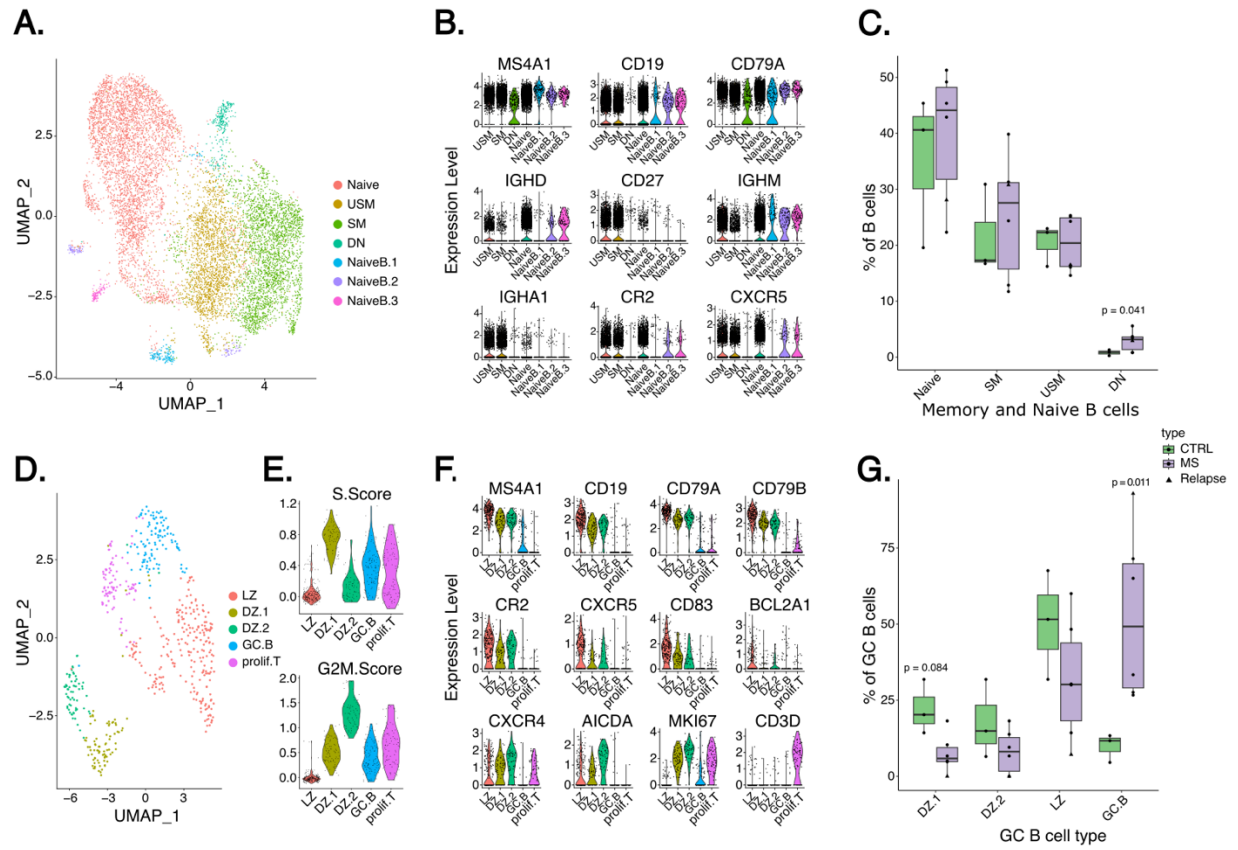
H.



1152 **Fig. 1. Skewed B and T cell populations in MS dcLNs highlighting enlarged**
1153 **memory B cell compartment**

1154 **(A)** Schematic diagram of study design, where the left panel illustrates sample collection
1155 including ultrasound-guided fine-needle aspirations (FNA) of deep cervical lymph nodes
1156 (dcLN). The right panel summarizes experiments performed for each subject. **(B)**
1157 Uniform Manifold Approximation and Projection (UMAP) of identified dcLN scRNA-seq
1158 cell clusters do not show a significant batch effect. **(C)** UMAP of identified cell clusters
1159 based on a combination of automatic annotation with SingleR (the Monaco reference)
1160 and manual annotation (in-house expertise) aided by the CITE-seq data. **(D-E)** Dotplot
1161 of key scRNA-seq (D) and CITE-seq (E) marker expression profiles in identified T and B
1162 cell subsets. **(F)** Bar plot of dcLN cell type proportions. **(G)** Box plot of cell type
1163 proportions in MS patients compared to controls using an unpaired t-test (p-values < 0.1
1164 are shown). The MS patient with an active relapse is highlighted with a triangle. **(H)** Bar
1165 plot of standardized Pearson residuals of cell subset numbers using Chi-squared test.
1166 Increased (red) and decreased (blue) cell subsets in MS patients' dcLNs are highlighted
1167 compared to healthy controls. Dashed red lines at ± 3.65 correspond to Bonferroni
1168 corrected p-values (< 0.00013) in the null distribution of standardized residuals.
1169 Abbreviations: GC, Germinal center; NK, Natural killer; PB, plasmablast; Tfh, T follicular
1170 helper, Tfr, T follicular regulator; T reg, regulatory T cell.

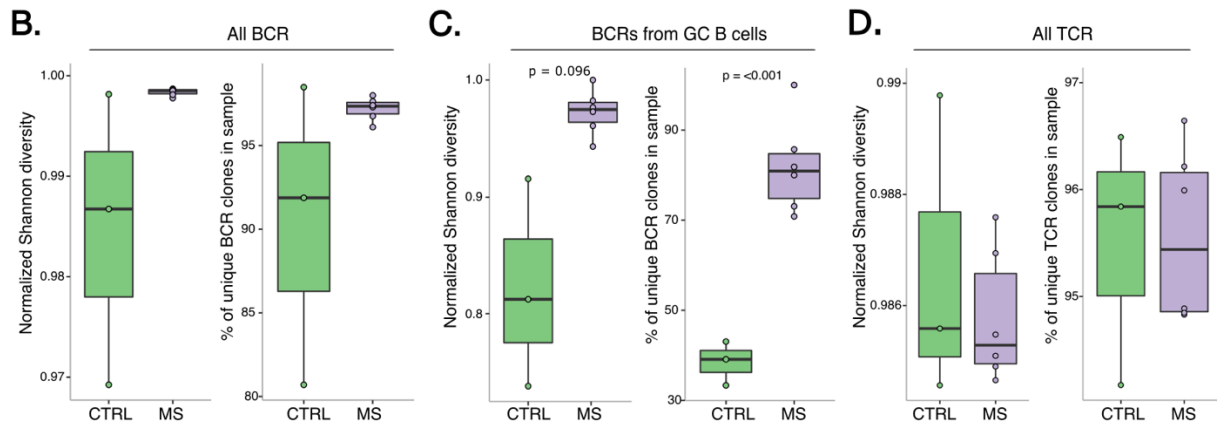
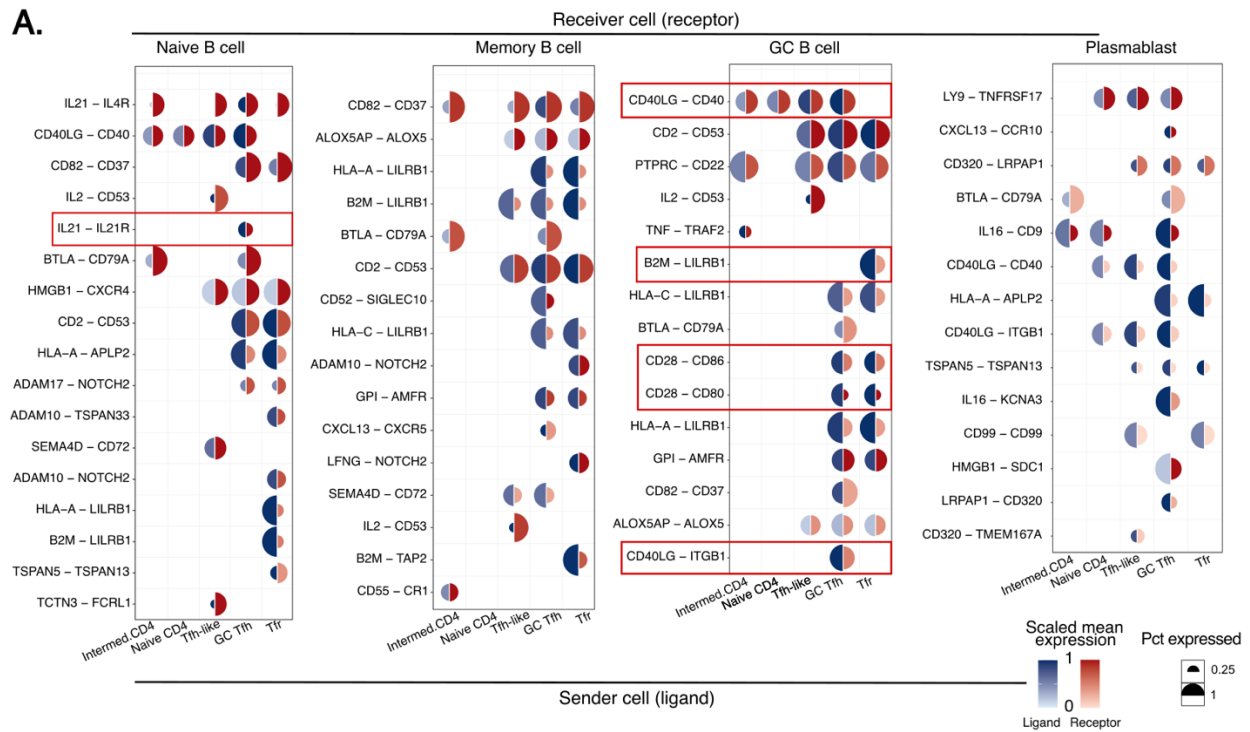
1171



1172

1173 **Fig. 2. Further analysis of the B cell compartment in MS dcLNs shows increased**
 1174 **double negative B cells**

1175 (A) UMAP of further clustered naïve and memory B cells. (B) Violin plot presenting the
 1176 expression of key transcripts used to identify naïve, switched memory (SM; IgD-,
 1177 CD27+), unswitched memory (USM; IgD+, CD27+), and double negative (DN) B cells.
 1178 (C) Box plot of memory and naïve B cell subsets (% of all B cells in a sample) between
 1179 MS patients compared to controls. (D) UMAP of further clustered GC B cells. (E) S
 1180 (upper panel) and G2M (lower panel) scores of GC B cell clusters were obtained using
 1181 Seurat. (F) Violin plot presenting the expression of key transcripts used to identify GC B
 1182 cell subsets: light zone (LZ), dark zone (DZ.1, DZ.2), and undefined GC B cell cluster
 1183 (GC.B). *CD3D* expression highlights proliferative T cells (prolif.T). (G) Box plot of GC B
 1184 cell subsets (% of all GC B cells in the sample) between MS patients and controls. In
 1185 (C) and (G), an unpaired t-test was used (p-values < 0.05 are shown), and the patient
 1186 with an active relapse is highlighted with a triangle.



1187

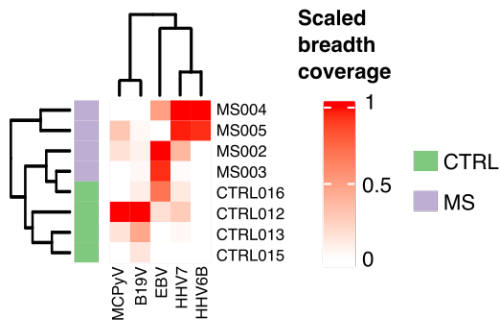
1188 **Fig. 3. GC BCRs in MS dLNs are less clonal**

1189 **(A)** Mushroom plot showing intercellular communication of helper T and Tfr cells
 1190 (ligand) between naïve, memory GC B cells and plasmablasts (receptor) using
 1191 NicheNet. The colour of red and blue corresponds to the scaled mean (from 0-1)
 1192 expression of ligand/receptor, while the size of the circle corresponds to a percentage of
 1193 cells expressing a particular transcript. Red rectangles highlight intercellular
 1194 communications emphasized in the Results. Diversity of **(B)** all BCRs, **(C)** BCRs of GC
 1195 B cells, and **(D)** all TCRs presented by boxplots from two different metrics of measuring

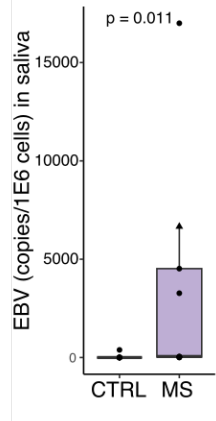
1196 repertoire diversity: normalized Shannon entropy (0 corresponds to monoclonal
1197 BCRs/TCRs, and 1 corresponds to all BCRs/TCRs would be diverse) and percent of
1198 unique clonotypes. In each case, an unpaired t-test was used to compare diversity
1199 estimates between MS patients and controls (p-values < 0.1 are shown with p-values <
1200 0.05 and < 0.1 considered significant and marginally significant respectively).
1201

1202

A.



B.

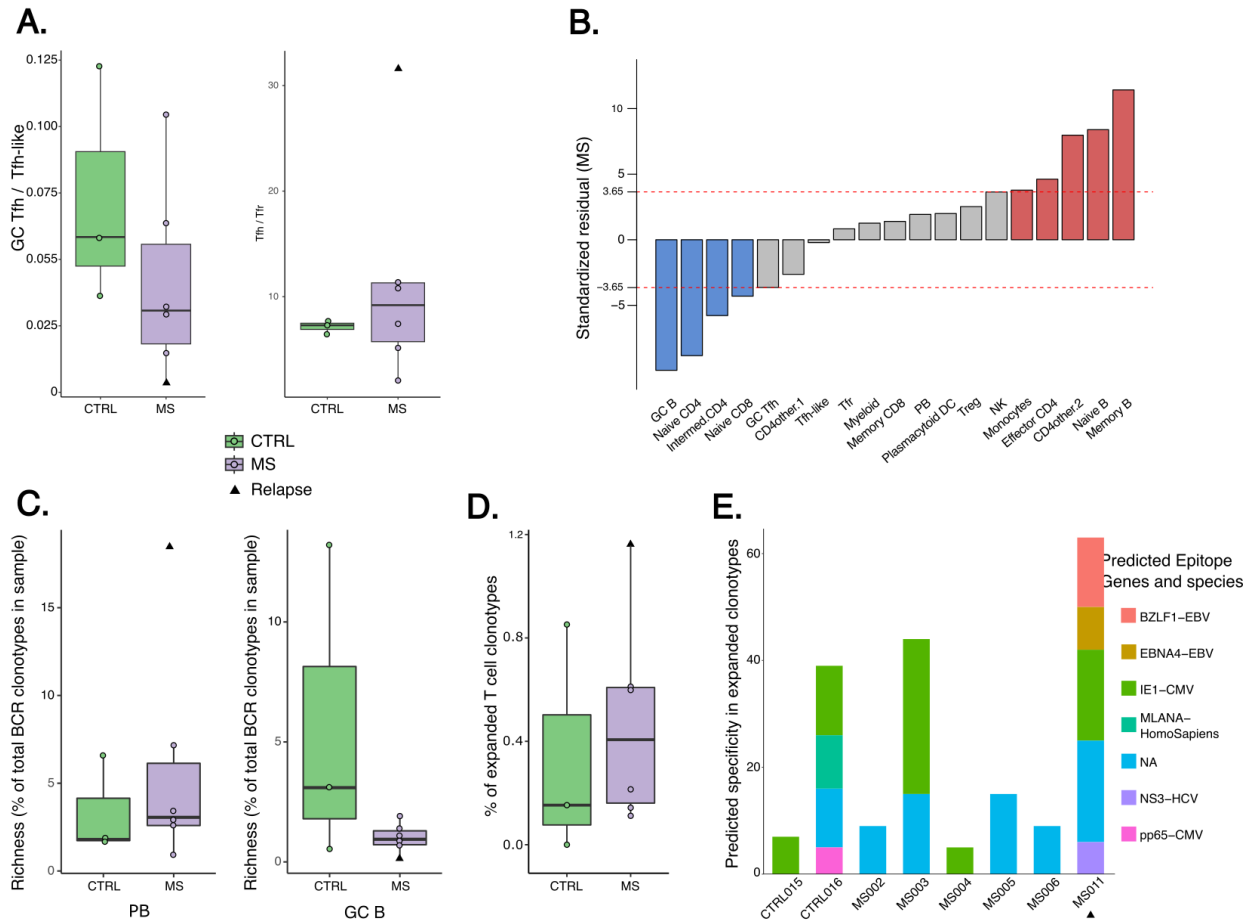


1202

1203 **Fig. 4. EBV, HHV-6B and HHV-7 show higher breadth coverage in dcLNs and EBV**
1204 **viral load is increased in MS patients compared to controls**

1205 (A) Heatmap illustrates the presence and the percentage of viral reads covering the
1206 EBV, HHV-6B, HHV-7, B19V, and MCPyV reference sequences (breadth coverage) in
1207 dcLNs determined using hybrid-capture sequencing. Viral breadth coverages were
1208 normalized from 0 to 1 separately for each virus, followed by agglomerative hierarchical
1209 clustering using Euclidean distance and Ward.D2 linkage. Dendrograms show the
1210 clustering of samples based on the breadth coverage profiles of the above-tested
1211 viruses. Negative samples for tested viruses are presented in white. (B) Box plot of EBV
1212 copies per 1 million cells in the saliva of MS patients compared to controls. EBV copy
1213 numbers were determined using qPCR. An unpaired t-test was used, and the patient
1214 with an active relapse is highlighted with a triangle.

1215



1216

1217 **Fig. 5. MS patient with an active relapse exhibits altered follicular cell ratios and**
 1218 **clonally expanded EBV targeting CD8+ T cells**

1219 **(A)** Box plots of GC Tfh / Tfh-like (left) and Tfh / Tfr ratios (right) in the MS patients
 1220 compared to healthy controls. Tfh is a sum of Tfh-like and GC Tfh cell counts. **(B)** Bar
 1221 plot of standardized Pearson residuals of cell subset numbers between controls and MS
 1222 patients without the patient with a relapse using Chi-squared test. Increased (red) and
 1223 decreased (blue) cell subsets in MS patients compared to healthy controls are
 1224 highlighted. Dashed red lines at ± 3.65 correspond to Bonferroni corrected p-values ($<$
 1225 0.00013) in the null distribution of standardized residuals. **(C)** Box plots of plasmablast
 1226 (left) and GC B cell (right) BCR richness (BCRs of total BCR clonotypes in each
 1227 sample). **(D)** Box plot of expanded T cell clonotypes of all T cell clones (%) in each
 1228 sample. **(E)** Stacked bar plot of predicted specificity in expanded T cell clonotypes. The

1229 VDJdb database was scanned for TCRab and b clonotypes using tcrdist3. In A and C-E,
1230 the patient with an active relapse is highlighted with a triangle.
1231

1232 **Table 1:** Characteristics of MS patients
1233

ID	Age	Sex	Other diseases	MS type	MRI Barkhoff	Time from onset (months)	Time from last relapse	Time from ivMP (months)	LN size (cm)	EDSS at sample collection	EDSS at 1 year follow up
MS001	20-29	M	asthma, pollen allergy	RRMS	4/4	8	8	-	2,06 X 0,63	0	0
MS002	40-49	M	no	RRMS	4/4	33	3	3	2,00 x 0,22	2.0	1.0
MS003	30-39	F	no	RRMS	3/4	4	4	-	NA	0	0
MS004	30-40	F	no	RRMS	3/5	4	4	-	NA	1	1
MS005	20-29	F	asthma, migrane, mild ankylosing spondylitis	RRMS	3/4	4	4	-	2.2 x 0.53	0	0
MS006	40-49	M	no	RRMS	3/4	75	6	6	NA	1.0	0
MS007	40-49	M	no	RRMS	4/4	36	3	3	1.04 X 0.58	2.5	5.0
MS010	30-39	F	no	PPMS	4/4	24	10	12	0.88 X 0.35	6.0	6.0
MS011	30-39	M	no	RRMS	4/4	48	0	-	1.85 X 0.58	3.5	2.0

1234

1235 Abbreviations: ivMP, intravenous methylprednisolone; EDSS, Expanded Disability

1236 Status Scale; LN, lymph node

1237
1238

Table 2: Results from the viral assays

ID	type	Plasma	Saliva (copies / 1*10 ⁶ cells)			cLN (breadth of coverage in %)				
		EBV VCA IgG (RU/ml)	EBV	HHV6B	HHV7	EBV	HHV-6B	HHV-7	MCPyV	B19V
CTRL008	CTRL	0	0	82	32400					
CTRL009	CTRL	104,59	387	132	77,1					
CTRL012	CTRL	151	0	0	347	5,13	0	26,4	22.4	89,5
CTRL013	CTRL	63,5	0	17,9	2210	0	0	3,8	3.4	41,2
CTRL014	CTRL	137	0	38,2	525					
CTRL015	CTRL	146,3	0	334	25300	0	0	0	0	12,3
CTRL016	CTRL		0	491	211000	20,8	0	11,4	0	8,4
MS001	MS	172,86	3270	33,8	2030					
MS002	MS	136,26	52,8	314	375	29,9	0	36,8	3,5	6,2
MS003	MS	179,04	0	69,2	11800	28,2	0	1,84	0	3,1
MS004	MS	223,73	26,2	297	3680	14,7	10,12	98,6	0	0
MS005	MS	194,59	17000	219	74100	0	9,5	95,67	6,7	3,5
MS006	MS	179,72	4520	0	221					
MS007	MS	209,72	10,4	15,2	2350					
MS010	MS	153,48	37	0	1890					
MS011	MS	177,19	6660	389	154000					

1239
1240
1241
1242

Abbreviations: EBV, Epstein-Barr Virus; HHV, human herpes virus; MCPyV, Merkel cell polyomavirus; B19V, parvovirus B19